

Macroscopic effects of an anisotropic Gaussian-type repulsive potential: nematic alignment and spatial effects

Sara Merino-Aceituno* Steffen Plunder† Claudia Wytrzens* Havva Yoldaş‡§

October 10, 2024

Abstract

Elongated particles in dense systems often exhibit alignment due to volume exclusion interactions, leading to packing configurations. Traditional models of collective dynamics typically impose this alignment phenomenologically, neglecting the influence of volume exclusion on particle positions. In this paper, we derive nematic alignment from an anisotropic repulsive potential, focusing on a Gaussian-type potential and first-order dynamics for the particles. By analyzing larger particle systems and performing a hydrodynamic limit, we uncover the effects of anisotropy on both particle density and direction. Our findings reveal that while particle density evolves independently of direction, anisotropy slows down nonlinear diffusion. The direction dynamics are affected by the particles' position and involve complex transport and diffusion processes, with different behaviors for oblate and prolate particles. The key to obtaining these results lies in recent advancements in Generalized Collision Invariants offered by Degond, Frouvelle and Liu (KRM 2022) in [14].

Contents

1	Introduction	2
1.1	Volume exclusion and nematic alignment	2
1.2	A discrete model for anisotropic particles	3
1.3	Kinetic equation and macroscopic quantities	6
2	Continuum equations	7
2.1	Properties of the operator C	9
2.2	The macroscopic limit	12
2.3	Comments on the continuum equations	14
2.3.1	The equation for the mass density	14
2.3.2	The equation for the mean-nematic direction	15
2.3.3	The case $a = 2$	16
2.4	Parameter regime for the validity of the continuum equations	17

*Faculty of Mathematics, University of Vienna, Oskar-Morgenstern-Platz 1, 1090 Vienna, Austria.
sara.merino@univie.ac.at & claudia.wytrzens@univie.ac.at

†Institute for the Advanced Study of Human Biology (ASHBi), KUIAS, Kyoto University, Faculty of Medicine Bldg. B, Kyoto, 606-8303, Japan. plunder.steffen.2a@kyoto-u.ac.jp

‡Delft Institute of Applied Mathematics, Faculty of Electrical Engineering, Mathematics and Computer Science, Delft University of Technology, Mekelweg 4, 2628CD Delft, The Netherlands. h.yoldas@tudelft.nl

§Theoretical Sciences Visiting Program (TSVP), Okinawa Institute of Science and Technology Graduate University, Onna, 904-0495, Japan. havva-yoldas@oist.jp

Keywords and phrases. Anisotropic Gaussian-type repulsive potential, nematic alignment, mean-field limit, continuum equations, kinetic equations, Berne-Pechukas potential, prolate and oblate particles

2020 Mathematics Subject Classification. 35Q92, 82C22, 82D30, 82B40

3	Repulsive potentials and particle simulations	19
3.1	Gaussian-type anisotropic repulsive potentials	19
3.1.1	Motivation for the interaction potential	19
3.2	Numerical simulations	20
3.2.1	Numerical implementation	20
3.2.2	Parameter study	21
3.2.3	Simulation results	22
3.2.4	Numerical comparison of the potentials	25
4	Proof of Theorem 2.16	26
4.1	Preliminaries	27
4.2	Limit for f^ε	28
4.3	Derivation of Equation (2.17a)	29
4.4	Derivation of Equation (2.17b).	29
4.4.1	Limit of the terms not involving B_f	30
4.4.2	Limit of the term with B_f	33
5	Conclusions	37
A	Appendices	38
A.1	Proof of Lemma 2.1	38
A.2	Proof of Lemma 4.2	39
A.3	Numerical approximation of $K(\eta)$ and additional figures	39

1 Introduction

Volume exclusion interactions play a central role in many physical and biological systems. In particular, they are fundamental in explaining emergent patterns like swarming [32], and spontaneous alignment of anisotropic particles [22]. The latter is called *nematic alignment*. The term *nematic* indicates that the alignment takes place in a given direction (not necessarily in a given orientation): if $u_1, u_2 \in \mathbb{R}^n$ are such that $|u_1| = |u_2| = 1$, we say that the two vectors are *nematically* aligned if $u_1 = \pm u_2$. Nematic alignment is sometimes referred to as *apolar* alignment since it is in contrast to *polar* alignment which requires $u_1 = u_2$. Some examples of nematic alignment can be found in suspensions of rod-like particles in high-densities [3], and biological systems like myxobacteria [18].

1.1 Volume exclusion and nematic alignment

Various volume exclusion models have been proposed to investigate cell dynamics, such as the vertex model [1, 23, 25] and other packing systems [13]. However, most agent-based models consider the agents as point-particles and impose phenomenological behavior that is assumed to be caused by volume exclusion interactions. Particularly, in most of these mathematical models for collective dynamics, the particle alignment is imposed via a force term without dealing with the contact interactions directly, see, e.g., [17, 18, 21].

Typical models for collective dynamics with nematic alignment take the following shape: agents move at a constant speed and try to align their direction of motion with one of their neighbors up to some noise. Specifically, we consider N agents who are identified by their positions $X_i \in \mathbb{R}^n$, $n \in \{2, 3\}$

and their directions $u_i \in \mathbb{S}^{n-1}$ on the $n - 1$ -dimensional sphere. Then their dynamics are governed by

$$dX_i = v_0 u_i dt, \quad (1.1a)$$

$$du_i = \frac{1}{N} \sum_{j=1}^N K(|X_i - X_j|) \nabla_{u_i} V_{\text{nem}}(u_i, u_j) dt + P_{u_i^\perp} \circ \sqrt{2D_u} dB_i, \quad (1.1b)$$

$$V_{\text{nem}}(u_i, u_j) := \lambda(u_i \cdot u_j)^2, \quad (1.1c)$$

where ∇_{u_i} is the gradient on the sphere, $V_{\text{nem}}(u_i, u_j)$ is the potential producing nematic alignment, $P_{u_i^\perp}$ is the orthonormal projection onto the orthonormal space to $u_i \in \mathbb{S}^{n-1}$, and $(B_i)_{i=1, \dots, N}$ are independent Brownian motions for $i = 1, \dots, N$. The stochastic differential equation (1.1b) must be understood in the Stratonovich sense. This is indicated with the symbol ‘ \circ ’ and it ensures that u_i remains on the sphere for all times where the solution is defined. The constant v_0 in (1.1a) is the speed of the particles and $D_u > 0$ in (1.1b) is the diffusion constant of the directions. Moreover, the function $K \geq 0$ is an interaction kernel measuring the influence of the potential force depending on the distance between particles. The constant $\lambda > 0$ describes the strength of the alignment force, which is expressed as the gradient flow dynamics of the potential $V_{\text{nem}} = V_{\text{nem}}(u_i, u_j)$. One can easily check that, indeed, the maximizer of this potential corresponds to $u_i = \pm u_j$, i.e., when two particles are *nematically* aligned. In this regard, we say that the model (1.1a)-(1.1c) imposes alignment for the particles. We refer the reader to, e.g., [15, 17–19, 24, 26], for models that use this approach or a similar one.

In the present work, we follow a different approach. We do not wish to impose alignment directly, but to investigate how it might emerge naturally from volume exclusion interactions. In particular, we study how volume exclusion interactions affect *both* the directions and the positions of the particles.

However, deriving continuum equations from agent-based models that undergo contact interactions is mathematically extremely challenging, see, e.g., [9, 10]. This is why up-to-date there is no rigorous coarse-graining for excluded volume dynamics starting from the first principles. Even in the widely-studied Boltzmann equation, the derivation from discrete dynamics (a particle system undergoing elastic collisions) is still unknown for large times [6]. For this reason, contact interactions are often approximated by using soft interaction potentials, like repulsive potentials, that produce active forces when two agents get closer than a given distance [7, 11, 20].

In this article, we focus on a particular repulsive potential that is used for simulating the interactions of anisotropic particles: the Gaussian repulsive potential [5] for elliptic (dimension $n = 2$) or spheroidal (dimension $n = 3$) particles, see Figure 1. For related works in the biophysics literature see, e.g., [3, 4].

Our goal is to investigate for which shape of the Gaussian potential we obtain an alignment force for the continuum equation, and what is the effect of this force on the positions of the particles. The reason for the last point is that in classical models for nematic alignment, the potential only modifies the direction of motion of the agents, but not their positions. One can expect that, from interaction forces, agents may *push* each other modifying their positions. The question of interest here is what effect this *pushing* has on the positions of the particles.

1.2 A discrete model for anisotropic particles

In this article, we study particles with either elliptic shape in the case of dimension $n = 2$ or spheroidal shape for dimension $n = 3$ (see Figure 1). In both cases, the particles are identical and are identified by their center $X \in \mathbb{R}^n$, the direction of one of the axes specified by a unit vector $u \in \mathbb{S}^{n-1}$, and the lengths of the major and minor axes. In dimension $n = 2$, u denotes the direction of the major axis whose length is $\ell \geq 0$ and the length of the minor axis is denoted by $d \geq 0$. In dimension $n = 2$, the *main axis* is the principal axis, i.e., the axis with longer length; whereas in dimension $n = 3$, the main axis is the axis of rotation.

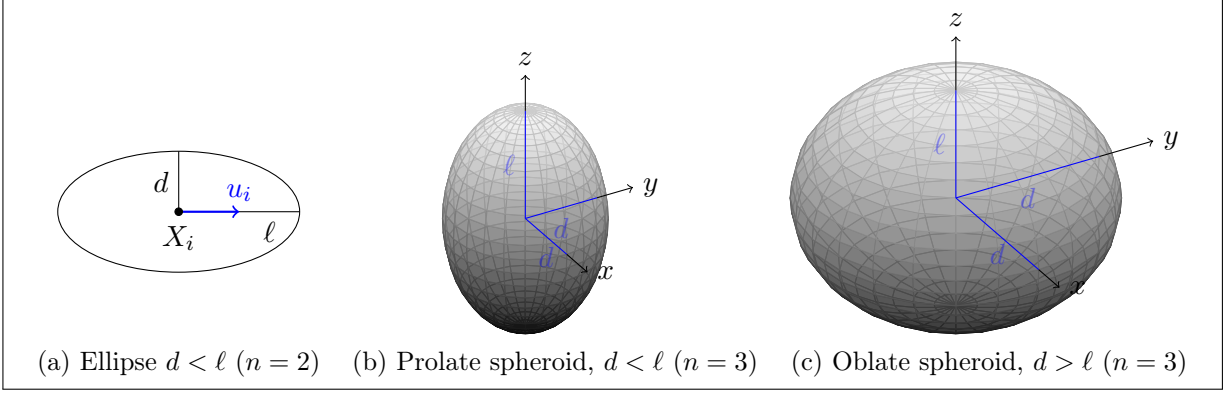


Figure 1: Spheroids are obtained by rotating an ellipse, shown in (a), around one of its principal axes. If the revolution is around the major axis, the spheroid is called prolate (b); if it is around the minor axis, it is called oblate (c).

We define the constant χ to characterize the shape of ellipses and spheroids,

$$\chi := \frac{\ell^2 - d^2}{\ell^2 + d^2}, \quad (1.2)$$

which measures the anisotropy of particles. In dimension $n = 2$, we have that $\chi \in [0, 1]$. In this case, $\chi = 0$ and $\chi = 1$ correspond to circular and rod-shaped particles, respectively. In dimension $n = 3$, we have $\chi \in [-1, 1]$. In this case, the negative values of χ correspond to oblate particles (rotation around the minor axis), and the positive values of χ correspond to prolate particles (rotation around the major axis); see Figure 1. In particular, $\chi = 0$ corresponds to spheres; $\chi = -1$ to infinitely flat disks; and $\chi = 1$ to infinitely thin rods.

We consider N identical particles identified by their centers $X_i \in \mathbb{R}^n$ and the direction of their main axes $u_i \in \mathbb{S}^{n-1}$ (notice that this is not uniquely defined as u_i and $-u_i$ prescribe the same direction) for $i = 1, \dots, N$. Two particles (X_i, u_i) , (X_j, u_j) are said to be (nematic) aligned when $u_i = \pm u_j$. For simplicity, here we consider only inert particles, i.e., $v_0 = 0$. However, this could be easily extended.

We assume that the repulsive potential V_b acts on the distance between the centers of two particles $X_j - X_i$ and the directions of their main axes u_i, u_j , i.e., $V_b(u_i, u_j, X_j - X_i)$. The model follows the steepest gradient descent of the potential V_b together with some noise both in the positions of the centers and in the directions of the main axes and it is given by

$$dX_i = -\mu \frac{1}{N} \sum_{j=1}^N \nabla_{X_i} V_b(u_i, u_j, X_j - X_i) dt + \sqrt{2D_x} dB_i, \quad (1.3a)$$

$$du_i = -\lambda \frac{1}{N} \sum_{j=1}^N \nabla_{u_i} V_b(u_i, u_j, X_j - X_i) dt + P_{u_i^\perp} \circ \sqrt{2D_u} d\tilde{B}_i, \quad (1.3b)$$

where ∇_{u_i} and $P_{u_i^\perp}$ are the same as before, B_i, \tilde{B}_i are independent Brownian motions for $i = 1, \dots, N$; and μ, λ, D_x, D_u are positive constants. The potential V_b corresponds to an anisotropic repulsive potential. In [8], the authors propose a model to describe the motion of spheroidal particles that are suspended in an incompressible fluid. The system (1.3a)-(1.3b) can be seen as the overdamped regime for these equations when there is no fluid.

In particular, notice that the potential V_b acts also on the distance between the centers of the particles. This effect does not appear in the classical nematic-alignment model (1.1a)-(1.1c). Our goal is to investigate how this potential affects the mean-nematic direction and the positions of the particles.

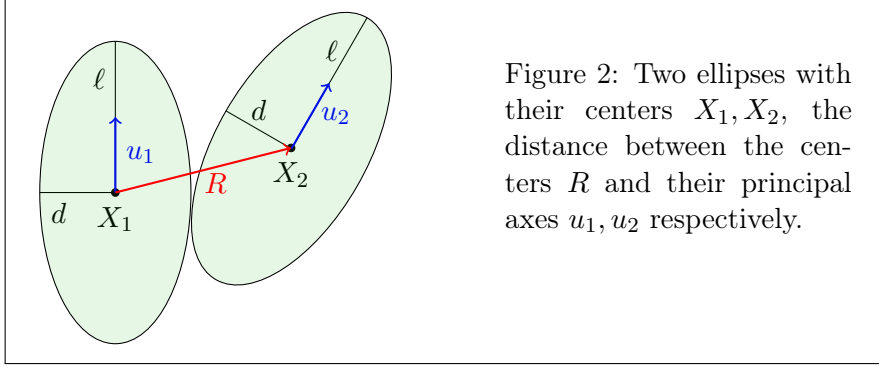


Figure 2: Two ellipses with their centers X_1, X_2 , the distance between the centers R and their principal axes u_1, u_2 respectively.

To carry this out, we derive a kinetic equation (see Section 1.3) for system (1.3a)-(1.3b) as a first step and subsequently we obtain continuum equations from the kinetic equation (see Section 2).

Let us have a closer look at the interaction potential. We describe the binary interactions between identical particles (ellipses for $n = 2$, or spheroids for $n = 3$, see Figures 1 and 2) via an anisotropic Gaussian-type potential V_b of the form

$$V_b(u_1, u_2, R) = (4\pi)^{-n/2} b(u_1, u_2) \exp(-R^T \Sigma^{-1} R), \quad (1.4)$$

where $b(u_1, u_2) \geq 0$ is a scaling factor, $R = X_2 - X_1$ is the vector between the centers of two particles, and the over index ‘T’ denotes the vector transpose. The matrix Σ is given by

$$\Sigma = \gamma_1 + \gamma_2,$$

where

$$\gamma_i = (\ell^2 - d^2) u_i \otimes u_i + d^2 \text{Id}, \quad i \in \{1, 2\}.$$

Our particular choice of the scaling factor b is given by

$$b_{\text{WG}}(u_1, u_2) := (1 - \chi^2 (u_1 \cdot u_2)^2)^{1/2} = \det(\Sigma)^{1/2}. \quad (1.5)$$

Using the scaling factor (1.5), the weighted Gaussian potential (1.4) takes the following form:

$$V_{\text{bWG}}(u_1, u_2, R) := (4\pi)^{-n/2} \det(\Sigma)^{1/2} \exp(-R^T \Sigma^{-1} R). \quad (1.6)$$

We dedicate Section 3.1 to a detailed explanation of repulsive potentials and some numerical simulations to show their effect on the dynamics of interacting particles. This section also includes a more detailed motivation for our particular choice of the scaling factor (1.5). Before we explain the kinetic equation arising from the particle dynamics, we make the following remark:

Remark 1.1. In [5], Berne and Pechukas considered the potential U for a single spheroid with its center x and direction of its main axis u :

$$U(x) := \exp(-x^T \gamma^{-1} x),$$

where $\gamma = (\ell^2 - d^2) u \otimes u + d^2 \text{Id}$. Using the potential $U = U(x)$, they introduced the anisotropic Gaussian-type potential (1.4) to describe the binary repulsive interactions. The level sets where U is constant correspond to ellipsoids of revolution about the axis u , i.e., spheroids concentric to the original (x, u) -spheroid, and they remain so even if the potential U is multiplied by a factor that could potentially depend on u . For this reason, introducing the scaling factor $b = b(u_1, u_2)$ does not change the intrinsic properties of the potential. On the other hand, this offers some simplifications for mathematical analysis, see Section 3.1 for more details.

1.3 Kinetic equation and macroscopic quantities

In this section, we write the mean-field equation (or large-particle limit) of the particle system (1.3a)-(1.3b). We consider a system of $N \geq 0$ identical particles in \mathbb{R}^n for $n \in \{2, 3\}$, identified by the positions of their centers and the directions of their main axes $(X_i, u_i)_{i=1, \dots, N}$ that follow the dynamics given by the system (1.3a)-(1.3b). As $N \rightarrow \infty$, the particle system is described by the probability distribution function $f = f(t, x, u)$ of particles at position x with the main axis in direction u at time t . Obtaining the equation for f , at least formally, uses standard tools from kinetic theory, which we will not detail here but refer the reader to, e.g., [29].

We start with defining an empirical measure f^N of the particles given by

$$f^N(t, x, u) = \frac{1}{N} \sum_{i=1}^N \delta_{(X_i(t), u_i(t))}(x, u), \quad (1.7)$$

where $\delta_{(X_i(t), u_i(t))}(x, u)$ is the Dirac delta distribution at $(X_i(t), u_i(t))$. The formal mean-field limit of the kinetic equation for the empirical distribution under the assumption that $f^N \rightarrow f$ as $N \rightarrow \infty$ solves

$$\partial_t f - \mu \nabla_x \cdot ((\nabla_x V_f) f) - \lambda \nabla_u \cdot ((\nabla_u V_f) f) - D_x \Delta_x f - D_u \Delta_u f = 0, \quad (1.8)$$

where

$$V_f(t, x_1, u_1) := \int_{\mathbb{S}^{n-1}} \int_{\mathbb{R}^n} V_b(u_1, u_2, x_2 - x_1) f(t, x_2, u_2) dx_2 du_2.$$

Next, we define the macroscopic quantities associated to $f = f(t, x, u)$, namely the spatial (or mass) density of the particles $\rho_f(t, x)$ and the mean-nematic direction $\Omega_f(t, x)$ at time $t \geq 0$ at position $x \in \mathbb{R}^n$. Our goal is to derive equations for $\rho_f(t, x)$ and $\Omega_f(t, x)$ from $f = f(t, x, u)$.

The mass density $\rho_f(t, x)$ is defined by

$$\rho_f(t, x) := \int_{\mathbb{S}^{n-1}} f(t, x, u) du.$$

To define $\Omega_f(t, x)$, we need to consider the following:

$$(\rho_f Q_f)(t, x) := \int_{\mathbb{S}^{n-1}} \left(u_2 \otimes u_2 - \frac{1}{n} \text{Id} \right) f(t, x, u_2) du_2. \quad (1.9)$$

where $Q_f(t, x)$ is a matrix associated to the distribution $f = f(t, x, u)$ and it is called *Q-tensor* in the literature of liquid crystals see, e.g., [2, 30]. Note that Q_f is a symmetric, trace-free matrix satisfying $Q_f \geq -\frac{1}{n} \text{Id}$.

The principal eigenvector of $Q_f(t, x)$ gives the direction that corresponds to the mean-nematic direction of the particles located at $x \in \mathbb{R}^n$ at time $t \geq 0$ (see, e.g., page 15 of [16] for an explanation). We denote the principal eigenvector by $\Omega_f(t, x) \in \mathbb{S}^{n-1}$ as long as it is unique (up to a change of sign). We have, in particular, that $\Omega_f = \Omega_f(t, x)$ maximizes over \mathbb{S}^{n-1} the quantity (see page 37 of [16]),

$$u \mapsto u \cdot (\rho_f Q_f) u = \int_{\mathbb{S}^{n-1}} \left((u \cdot u_2)^2 - \frac{1}{n} \right) f(t, x, u_2) du_2.$$

This can also be seen as a consequence of the Courant-Fisher theorem, or the min-max theorem, see, e.g., [28]. Indeed, notice that if $f = f^N$ is the empirical measure (1.7), the previous expression implies that Ω_f maximizes

$$u \mapsto \frac{1}{N} \sum_{j=1}^N (u \cdot u_j)^2,$$

which is analogous to maximizing

$$\frac{1}{N} \sum_{j=1}^N V_{\text{nem}}(u, u_j),$$

where V_{nem} is the potential given in Equation (1.1c). Thus, Ω_f defined in this way is indeed the mean-nematic direction.

In this article, we derive equations for the spatial density $\rho = \rho_f(t, x)$ of particles and their mean-nematic direction $\Omega = \Omega_f(t, x)$. Before delving into the details in the next section, we end this introductory part with some comments on the continuum equations. For the density ρ , we obtain an equation of the form

$$\partial_t \rho = D_x \Delta_x \rho + \mu \nabla_x \cdot (K(\rho) \rho \nabla_x \rho),$$

where K is a functional that depends on ρ . Notice that the particle density does not depend on the mean-nematic direction Ω . However, the effect of the repulsive potential is present through the functional K , which depends, particularly, on the anisotropy parameter χ^2 (defined in (1.2)).

The equation for Ω is a combination of transport and diffusion, with a cross-diffusion term in ρ . Intriguingly, the well-posedness of the equation imposes a constraint on the parameters. Particularly, we require that

$$\frac{D_x}{\mu} > \frac{D_u}{\lambda}. \quad (1.10)$$

However, this constraint is not required at the particle level. We discuss in detail possible explanations for this constraint in Section 2.3. Our main result is given in Theorem 2.16 and its interpretation is given in Section 2.3.

Structure of the paper. In Section 2, we state our main result, Theorem 2.16, after some preliminary definitions and results. Theorem 2.16 is followed by an extensive interpretation section, Section 2.3, where we comment on each component of our continuum equations. In Section 3.1, we motivate our choice of the Gaussian-type repulsive potential (1.6) by comparing it with similar interaction potentials used in the literature. Section 3.2 is dedicated to numerical simulations of the stochastic particle system (1.3a)-(1.3b). Here, we conduct a detailed parameter study and a numerical comparison of the effect of different repulsive potentials on the global alignment of the particles. We dedicate Section 4 to the proof of Theorem 2.16. Finally, the paper is complemented with some concluding remarks and perspectives in Section 5, followed by appendices.

2 Continuum equations

In this section, we derive continuum equations, namely the equations for the mass density $\rho_f(t, x)$ and the mean-nematic direction $\Omega_f(t, x)$ from the kinetic equation (1.8). We start with non-dimensionalizing the kinetic equation (1.8). To this end, we introduce a scaling parameter $0 < \varepsilon \ll 1$ and denote by f^ε the solution of the scaled kinetic equation.

Non-dimensionalization. Introducing the units of space x_0 and time t_0 , we define the dimensionless variables,

$$\tilde{x} = \frac{x}{x_0}, \quad \tilde{t} = \frac{t}{t_0}, \quad \tilde{f} = f x_0^n,$$

and the dimensionless parameters,

$$\tilde{\mu} = \mu \frac{t_0}{x_0^2}, \quad \tilde{\lambda} = t_0 \lambda, \quad \tilde{D}_u = t_0 D_u, \quad \tilde{D}_x = \frac{D_x t_0}{x_0^2}, \quad \tilde{\ell} = \frac{\ell}{x_0}, \quad \tilde{d} = \frac{d}{x_0}.$$

We remark that the anisotropy factor χ and the potential V_b are already dimensionless. Thus, we have

$$\tilde{\chi} = \chi, \quad \tilde{V}_b = V_b, \quad \tilde{V}_f = V_f.$$

Using these dimensionless quantities, dropping the tildes for the sake of simplicity, we obtain exactly the same equation as before, i.e., we end up with Equation (1.8). But now all the variables and parameters are without units.

Scaling. Considering a scaling parameter $0 < \varepsilon \ll 1$, we introduce the primed variables below,

$$\ell = \varepsilon \ell', \quad d = \varepsilon d', \quad \mu = \varepsilon^{-n} \mu', \quad \lambda = \varepsilon^{-(n+a)} \lambda', \quad D_u = \varepsilon^{-a} D'_u,$$

where $a \in (0, 2]$ is a constant. Notice that the scaling in ℓ and d combined with the scaling of the potential by $\varepsilon^n V_f^\varepsilon = V_f$ produces a localization in space of the potential V_f (for details, see Lemma 2.1). The choice of a has an influence on the resulting macroscopic equation (see Remark 2.2). Notice also that the diffusion constant D_x stays of order 1. We obtain the following rescaled kinetic equation (skipping the primes for simplicity):

$$\partial_t f^\varepsilon - \mu \nabla_x \cdot ((\nabla_x V_{f^\varepsilon}^\varepsilon) f^\varepsilon) - D_x \Delta_x f^\varepsilon = \frac{1}{\varepsilon^a} (\lambda \nabla_u \cdot ((\nabla_u V_{f^\varepsilon}^\varepsilon) f^\varepsilon) + D_u \Delta_u f^\varepsilon).$$

Next, we further expand the potential V_f .

Lemma 2.1 (Expansion of the potential). *Considering $\ell = \varepsilon \ell'$ and $d = \varepsilon d'$ we have the following expansion V_f^ε of the scaled weighted Gaussian potential V_f (defined by using (1.6)):*

$$\begin{aligned} V_f^\varepsilon(t, x_1, u_1) &:= \frac{1}{\varepsilon^n} V_f(t, x_1, u_1) = \int_{\mathbb{S}^{n-1}} (1 - \chi^2(u_1 \cdot u_2)^2) f(t, x_1, u_2) du_2 \\ &\quad + \frac{\varepsilon^2}{4} \int_{\mathbb{S}^{n-1}} (1 - \chi^2(u_1 \cdot u_2)^2) \Sigma(u_1, u_2) : D_x^2 f(t, x_1, u_2) du_2 + \mathcal{O}(\varepsilon^3) \\ &= W_f(t, x_1, u_1) + \varepsilon^2 B_f(t, x_1, u_1) + \mathcal{O}(\varepsilon^3), \end{aligned} \quad (2.1)$$

where D_x^2 is the Hessian, i.e., a $n \times n$ -matrix with components $(D_x^2)_{ij} = \partial_{x_i} \partial_{x_j}$, ‘:’ denotes the double contraction, i.e., $A : B := \sum_{i,j} A_{ij} B_{ij}$, W_f and B_f are defined as

$$W_f(t, x_1, u_1) := \int_{\mathbb{S}^{n-1}} (1 - \chi^2(u_1 \cdot u_2)^2) f(t, x_1, u_2) du_2, \quad (2.2)$$

$$B_f(t, x_1, u_1) := \frac{1}{4} \int_{\mathbb{S}^{n-1}} (1 - \chi^2(u_1 \cdot u_2)^2) \Sigma(u_1, u_2) : D_x^2 f(t, x_1, u_2) du_2. \quad (2.3)$$

Proof. The proof can be found in Appendix A.1. □

Nematic alignment potentials analogous to W_f appear in the literature of collective dynamics, e.g., in a model for nematic alignment of fibers [12], in a model for body attitude coordination [16], and in a model of pure nematic alignment [19].

Finally, using the expansion for the scaled weighted Gaussian potential V_f^ε in Lemma 2.1 we obtain:

$$\partial_t f^\varepsilon - \mu \nabla_x \cdot ((\nabla_x W_{f^\varepsilon}) f^\varepsilon) - D_x \Delta_x f^\varepsilon - \varepsilon^{2-a} \lambda \nabla_u \cdot ((\nabla_u B_{f^\varepsilon}) f^\varepsilon) = \frac{D_u}{\varepsilon^a} C(f^\varepsilon) + \mathcal{O}(\min(\varepsilon^2, \varepsilon^{3-a})), \quad (2.4)$$

with $a \in (0, 2]$ and where

$$C(f) := \frac{\lambda}{D_u} \nabla_u \cdot ((\nabla_u W_f) f) + \Delta_u f.$$

Remark 2.2 (Motivation for the scaling factor a). The scaled kinetic equation with $a = 2$ can also be equivalently obtained by just scaling space and time by $x' = \sqrt{\varepsilon}x$ and $t' = \varepsilon t$, which is a more natural scaling choice. However, we also consider an alternative scaling where the term B_f vanishes in the macroscopic limit. The term B_f is specific to the Gaussian repulsive potential, and it acts as a correction to the primary nematic alignment potential W_f . As we will see, the term B_f is unique in the sense that it gives different behavior for prolate and oblate particles (see term Π_3 in the macroscopic limit (2.21)). In the specific case where $a \in (0, 2)$, the term B_f disappears in the limit. The two scaling factors that we consider highlight the differences in the dynamics with and without the term B_f . Thus, $a = 2$ can be viewed as a diffusive scaling, while $a \in (0, 2)$ represents a generalized scaling law distinct from hyperbolic scaling.

Our goal is to derive equations for the time evolution of the mass density $\rho_f = \rho_f(t, x)$ and the mean-nematic direction $\Omega_f = \Omega_f(t, x)$. For this reason, we rewrite the kinetic equation in terms of the Q -tensor Q_f . First, using that $(u \cdot v)^2 = u^T (v \otimes v) u$ and that $\rho_f = \int_{\mathbb{S}^{n-1}} f \, du$, we rewrite W_f in (2.2) as follows:

$$W_f(t, x_1, u_1) = -\chi^2 u_1^T (\rho_f Q_f) u_1 - \left(\frac{\chi^2}{n} - 1 \right) \rho_f. \quad (2.5)$$

With this new expression for W_f and using that $\nabla_u \rho_f = 0$, the kinetic equation (2.4) becomes

$$\begin{aligned} \partial_t f^\varepsilon + \mu \chi^2 \nabla_x \cdot (\nabla_x (u^T (\rho_{f^\varepsilon} Q_{f^\varepsilon}) u) f^\varepsilon) + \mu \left(\frac{\chi^2}{n} - 1 \right) \nabla_x \cdot ((\nabla_x \rho_{f^\varepsilon}) f^\varepsilon) \\ - \lambda \varepsilon^{2-a} \nabla_u \cdot ((\nabla_u B_f) f^\varepsilon) - D_x \Delta_x f^\varepsilon = \frac{D_u}{\varepsilon^a} C(f^\varepsilon) + \mathcal{O}(\min(\varepsilon^2, \varepsilon^{3-a})), \end{aligned} \quad (2.6)$$

where

$$C(f) = \nabla_u \cdot \left(\nabla_u f - \frac{\lambda}{D_u} f \nabla_u (\chi^2 u^T (\rho_f Q_f) u) \right). \quad (2.7)$$

In the next section, we give some preliminary definitions and concepts to analyze the operator C in detail.

2.1 Properties of the operator C

From Equation (2.6), we can already observe that, at least formally, if f^ε converges to some function f^0 as $\varepsilon \rightarrow 0$, then it must hold that f^0 belongs to the kernel of the operator C , i.e., $C(f_0) = 0$. Fortunately, the equilibria for C have already been studied in [14] and in this section we summarize the results presented there. Therefore, this section mainly follows some results of [14] omitting their proofs.

In particular, we are interested in stable equilibria of the operator C (for an exact notion of stability see [14]). The key result, containing the characterization of the stable equilibria of C , is given in Lemma 2.10, which can be found at the end of this section.

Remark 2.3. The operator C defined in (2.7) is equivalent to the one presented in Equation (39) in [14] for

$$\alpha := \frac{\chi^2 \lambda}{D_u}. \quad (2.8)$$

Next, we introduce some preliminaries.

Definition 2.4 (Uniaxial tensor). Given $\Omega \in \mathbb{S}^{n-1}$, the normalized, uniaxial, trace-free tensor A_Ω in the direction of Ω is defined by

$$A_\Omega = \Omega \otimes \Omega - \frac{1}{n} \text{Id}. \quad (2.9)$$

The tensor A_Ω is symmetric with principal eigenvalue $\frac{n-1}{n}$. It is called *uniaxial* since it has only two eigenvalues and one of them is simple. The normalized eigenvectors associated to the simple eigenvalue are $\pm\Omega$.

Next, we define the Gibbs distributions of uniaxial tensors.

Definition 2.5 (Gibbs distribution of an uniaxial tensor). Given $\eta > 0$ and the tensor A_Ω , the Gibbs distribution $G_{\eta A_\Omega}$ associated to ηA_Ω is defined as

$$G_{\eta A_\Omega}(u) = \frac{1}{Z_\eta} e^{\eta(u \cdot \Omega)^2}, \quad \text{where} \quad Z_\eta = \int_{\mathbb{S}^{n-1}} e^{\eta(u \cdot \Omega)^2} du. \quad (2.10)$$

Finally, the order parameter associated to a Gibbs distribution is defined as follows.

Definition 2.6 (Order parameter). The order parameter associated to $G_{\eta A_\Omega}$ is denoted by $S_2 = S_2(\eta)$ and given by

$$S_2(\eta) := \frac{n}{n-1} \Omega^T Q_{G_{\eta A_\Omega}} \Omega = \frac{n}{n-1} \int_{\mathbb{S}^{n-1}} \left((u \cdot \Omega)^2 - \frac{1}{n} \right) G_{\eta A_\Omega} du, \quad (2.11)$$

where $Q_{G_{\eta A_\Omega}}$ is the Q -tensor associated to $G_{\eta A_\Omega}$.

Remark 2.7. Using the change of variables (4.1), the order parameter $S_2(\eta)$ can be written as

$$S_2(\eta) = \frac{n}{n-1} \int_0^\pi \left(\cos^2 \theta - \frac{1}{n} \right) g_\eta(\theta) \sin^{n-2} \theta d\theta. \quad (2.12)$$

where the function g_η is given in (4.2).

Notice that $S_2(\eta)$ is actually independent of Ω and it satisfies the following:

Lemma 2.8 (Proposition 2 in [14]). *It holds that*

$$Q_{G_{\eta A_\Omega}} = S_2(\eta) A_\Omega.$$

Moreover, $S_2 : (0, \infty) \rightarrow (0, 1)$ is non-decreasing with $S_2 \rightarrow 0$ as $\eta \rightarrow 0$ and $S_2 \rightarrow 1$ as $\eta \rightarrow \infty$.

Next, we define the function $\eta = \eta(\rho)$ implicitly through the following equation:

Proposition 2.9 (Implicit definition of $\eta = \eta(\rho)$, Proposition 3 in [14]). *The equation*

$$\frac{\eta}{\alpha \rho} = S_2(\eta) \quad (2.13)$$

has at least a root η if and only if $\rho \in (\rho_*, +\infty)$, $\rho_* > 0$. Moreover, (2.13) has at most two roots. Choosing the largest root, we can define a smooth, non-decreasing function $(\rho_*, +\infty) \rightarrow (\eta^*, +\infty)$, $\rho \mapsto \eta(\rho)$, where $\eta^* = \lim_{\rho \rightarrow \rho_*} \eta(\rho) \geq 0$.

Finally, with all the definitions above, we can state the main result regarding the equilibria of C :

Lemma 2.10 (Stable equilibria of C , Lemma 4.4 in [14]). *Let $n \in \{2, 3\}$. For ρ_* given in Proposition 2.9 the following holds:*

- (i). *If $\rho < \rho_*$, then $f = \rho$ (the uniform equilibrium) is the only stable equilibrium of the operator C .*
- (ii). *If $\rho > \rho_*$, then the only stable equilibria of the operator C are of the form*

$$f = \rho G_{\eta(\rho)A_\Omega}.$$

In particular, we have

$$Q_f = S_2(\eta(\rho))A_\Omega, \tag{2.14}$$

where S_2 and $\eta = \eta(\rho)$ are defined in (2.11) and (2.13) respectively. Equation (2.14) is referred to as ‘consistency relation’ and can be written, using (2.13), equivalently as

$$\alpha\rho Q_{G_{\eta(\rho)A_\Omega}} = \eta(\rho)A_\Omega. \tag{2.15}$$

Remark 2.11. The operator C is analogous to the operator that appears for models of nematic alignment where the nematic alignment is imposed, see, e.g., [19]. However, in [19] the potential is written in a so-called, ‘mean-field force’ form rather than a binary force. Here, we have the term

$$\varphi_1(u) := u^T \rho_f Q_f u = \int_{\mathbb{S}^{n-1}} \left((u \cdot u_2)^2 - \frac{1}{n} \right) f(t, x, u_2) du_2,$$

while in [19] this operator is replaced by

$$\varphi_2(u) := u^T A_{\Omega_f} u = (u \cdot \Omega_f)^2 - \frac{1}{n},$$

where Ω_f corresponds to the mean-nematic direction (that is why it is called ‘mean-field force’). We expect that both cases lead to nematic alignment. Already in the case φ_2 we see that $u = \pm\Omega_f$ is the maximizer. In the first case, we also know that Ω_f corresponds to the principal eigenvector of Q_f , gives the mean-nematic direction and maximizes φ_1 . However, it is not guaranteed that the principal eigenvalue has only multiplicity 1. This adds an extra degree of difficulty to the analysis. Lemma 2.10 demonstrates that this leads to phase transitions in the macroscopic limit, with spatial regions of disordered dynamics, i.e., the dynamics where a well-defined principal eigenvector does not exist, and thus, particles do not align. This takes place in the regions of low density, i.e., $\rho < \rho_*$.

Remark 2.12. Given the matrix Q_f , suppose that $\Omega_f \in \mathbb{S}^{n-1}$ is the principal eigenvector (assumed to be unique up to a change in sign). Then, it holds that A_{Ω_f} also has a principal eigenvector Ω_f . So, both Q_f and A_{Ω_f} give the same mean-nematic direction. However, $Q_f \neq A_{\Omega_f}$ in general. In particular, the principal eigenvalue of A_{Ω_f} is always $\frac{n-1}{n}$, while for Q_f the eigenvalues have $\frac{n-1}{n}$ as an upper bound (see [19]). In particular (see [14]), to measure the degree of nematic alignment one considers the following order parameter γ_f :

$$\gamma_f = \frac{n}{n-1} \beta_f \in (0, 1], \tag{2.16}$$

where β_f is the largest eigenvalue of Q_f . If f is uniformly distributed on the sphere (particles are fully misaligned), then γ_f is close to 0. On the contrary, if f is close to $\frac{1}{2}(\delta_\Omega + \delta_{-\Omega})$, i.e., particles are fully aligned and $Q_f = A_{\Omega_f}$, then $\gamma_f = 1$. So the case $Q_f = A_{\Omega_f}$ is an extreme case that corresponds to having all particles nematicallly aligned in the direction Ω_f .

In fact, the function $S_2 = S_2(\eta)$ is the order parameter of $G_{\eta A_\Omega}$.

Remark 2.13. As $\eta \rightarrow 0$, $G_{\eta A_\Omega}$ converges to the uniform probability distribution on \mathbb{S}^{n-1} and S_2 converges to 0. As $\eta \rightarrow \infty$, $G_{\eta A_\Omega}$ converges to two Dirac delta distributions $\frac{1}{2}(\delta_\Omega + \delta_{-\Omega})$ which accounts for fully aligned distribution in the direction of Ω and thus also S_2 converges to 1. Therefore, as η increases, S_2 increases too (see also Figure 10b), and $G_{\eta A_\Omega}$ shows increasing order of alignment.

Now, we are ready to state our main result in the next section.

2.2 The macroscopic limit

Assumption 2.14. *We assume throughout that all the functions are as smooth as needed so that all the limits exist and the convergences are as strong as needed.*

Next, we introduce the following definition which we will use in the theorem below.

Definition 2.15. Let A be a 5-tensor and B a 4-tensor in \mathbb{R}^n , then we define the following operation between tensors:

$$([A : B]_{[2,3,4,5;1,2,3,4]})_p := \sum_{j,k,l,m=1}^n A_{pjklm} B_{jklm}, \quad p = 1, \dots, n,$$

The contraction with the subscript $[2, 3 : 1, 2]$ is analogously defined.

We give our main result in the following theorem:

Theorem 2.16. *Let $n \in \{2, 3\}$, $a \in (0, 2]$, and $f^\varepsilon = f^\varepsilon(t, x, u)$ be the solution to the kinetic equation (2.6). Suppose that Assumption 2.14 holds and that $f^\varepsilon(t, x, u) \rightarrow f^0(t, x, u)$ as $\varepsilon \rightarrow 0$. Consider (t, x) such that $\int_{\mathbb{S}^{n-1}} f^0 du > \rho_*$ (where ρ_* is given in Proposition 2.9). Then, in this domain, it holds that $f^0 = \rho(t, x) G_{\eta(\rho) A_\Omega}$ with $\rho(t, x) = \int_{\mathbb{S}^{n-1}} f^0 du > \rho_*$, where $A_\Omega, G_{\eta(\rho) A_\Omega}, \eta(\rho)$ are given in (2.9), (2.10) and (2.13) respectively. Moreover, the mass density $\rho(t, x)$ and the mean-nematic direction of the particles $\Omega(t, x)$ satisfy the following system of equations*

$$\partial_t \rho = D_x \Delta_x \rho + \mu \nabla_x \cdot (K(\eta(\rho)) \rho \nabla_x \rho), \quad (2.17a)$$

$$\partial_t \Omega + \mu \Pi_2(\rho) (\nabla_x \rho \cdot \nabla_x) \Omega + \mu (\sigma - \nu) P_{\Omega^\perp} \Delta_x \Omega = \mathbb{1}_{a=2} \lambda \Pi_3(\Omega, \rho). \quad (2.17b)$$

where

$$K(\eta(\rho)) := 1 - \frac{\chi^2}{n} - \sigma \frac{n-1}{n} S_2(\eta(\rho)) \eta'(\rho), \quad (2.18)$$

and

$$\sigma := \frac{D_u}{\lambda}, \quad \nu := \frac{D_x}{\mu}.$$

Moreover, Π_2 is given by

$$\Pi_2(\rho) = \frac{\sigma - 2\nu}{\rho} + \frac{\chi^2}{n} - 1 + 2 \frac{\eta'(\rho)}{\eta(\rho)} (\sigma - \nu) + \eta'(\rho) \left(2(\sigma - \nu) \frac{c_{3,2}(\rho)}{c_{1,2}(\rho)} - d_{2,0}(\rho) (\sigma - 2\nu) - \frac{\sigma}{n} \right),$$

where, for $k, p \in \mathbb{N} \cup \{0\}$, $c_{k,p} = c_{k,p}(\rho)$ and $d_{k,p} = d_{k,p}(\rho)$ are given by

$$c_{k,p}(\rho) := \int_0^\pi \cos^k \theta g_{\eta(\rho)}(\theta) h_{\eta(\rho)}(\cos \theta) \sin^{n-2+p} \theta \, d\theta, \quad (2.19)$$

$$d_{k,p}(\rho) := \int_0^\pi \cos^k \theta g_{\eta(\rho)}(\theta) \sin^{n-2+p} \theta \, d\theta, \quad (2.20)$$

where the function h_η is defined in Proposition 4.5 and the function g_η is given in (4.2). It holds that $\frac{c_{3,2}}{c_{1,2}} \geq 0$ and $d_{2,0} \geq 0$.

In the case of $a = 2$, the right hand side of (2.17b) does not vanish and Π_3 is given by

$$\begin{aligned} \frac{8c_{1,2}(\rho)\eta(\rho)}{(n-1)}\Pi_3(\Omega, \rho) &= (\ell^2 - d^2)[(H_2^r : (D_x^2 \rho))]_{[2,3:1,2]} - 2\chi^2 d^2 [H_2^r : \Delta_x(\rho H_2)]_{[2,3:1,2]} \\ &\quad - \chi^2(\ell^2 - d^2) ([H_4^r : (D_x^2 \otimes (\rho H_2))]_{[2,3,4,5:1,2,3,4]} + [H_2^r \otimes D_x^2 : (\rho H_4)]_{[2,3,4,5:1,2,3,4]}) \end{aligned} \quad (2.21)$$

where in the case of dimension $n = 2$ we have that

$$H_2 = d_{2,0}(\Omega \otimes \Omega) + d_{0,2}(\Omega^\perp \otimes \Omega^\perp), \quad (2.22)$$

$$H_2^r = d_{2,2}\Omega^\perp \otimes \left((\Omega^\perp \otimes \Omega) + (\Omega \otimes \Omega^\perp) \right), \quad (2.23)$$

$$H_4 = d_{4,0}(\Omega \otimes \Omega \otimes \Omega \otimes \Omega) + d_{2,2}S_{2\Omega,2\Omega^\perp}(\Omega, \Omega^\perp) + d_{0,4}(\Omega^\perp \otimes \Omega^\perp \otimes \Omega^\perp \otimes \Omega^\perp), \quad (2.24)$$

$$H_4^r = \Omega^\perp \otimes \left(d_{4,2}S_{3\Omega,\Omega^\perp}(\Omega, \Omega^\perp) + d_{2,4}S_{\Omega,3\Omega^\perp}(\Omega, \Omega^\perp) \right), \quad (2.25)$$

with

$$\begin{aligned} S_{2\Omega,2\Omega^\perp}(\Omega, \Omega^\perp) &:= (\Omega \otimes \Omega^\perp + \Omega^\perp \otimes \Omega) \otimes (\Omega \otimes \Omega^\perp + \Omega^\perp \otimes \Omega) \\ &\quad + \Omega \otimes \Omega \otimes \Omega^\perp \otimes \Omega^\perp + \Omega^\perp \otimes \Omega^\perp \otimes \Omega \otimes \Omega, \end{aligned}$$

and

$$S_{3\Omega,\Omega^\perp}(\Omega, \Omega^\perp) := (\Omega \otimes \Omega) \otimes (\Omega \otimes \Omega^\perp + \Omega^\perp \otimes \Omega) + (\Omega \otimes \Omega^\perp + \Omega^\perp \otimes \Omega) \otimes (\Omega \otimes \Omega)$$

and $S_{\Omega,3\Omega^\perp}$ is defined analogously as $S_{3\Omega,\Omega^\perp}$ (by exchanging the values of Ω and Ω^\perp).

In dimension $n \geq 3$, the values of H_2, H_2^r, H_4, H_4^r are more complex and are given in Proposition 2.17 below.

Proposition 2.17 (Dimension $n \geq 3$). For $n \geq 3$ the functions H_2, H_2^r, H_4, H_4^r are given by

$$H_2(\eta, \Omega, \Omega^\perp) = d_{2,0}(\Omega \otimes \Omega) + \frac{d_{0,2}}{n-1}P_{\Omega^\perp} \quad (2.26)$$

$$H_2^r(\eta, \Omega, \Omega^\perp) = \frac{d_{2,2}}{n-1} (P_{\Omega^\perp} \otimes \Omega + [P_{\Omega^\perp} \otimes \Omega \otimes P_{\Omega^\perp}]_{:24}) \quad (2.27)$$

$$\begin{aligned} H_4(\eta, \Omega, \Omega^\perp) &= d_{4,0}(\Omega \otimes \Omega \otimes \Omega \otimes \Omega) + \frac{d_{0,4}}{(n-1)(n+1)}\Gamma \\ &\quad + \frac{d_{2,2}}{n-1} \left(P_{\Omega^\perp} \otimes \Omega \otimes \Omega + \Omega \otimes P_{\Omega^\perp} \otimes \Omega + \Omega \otimes \Omega \otimes P_{\Omega^\perp} \right. \\ &\quad \left. + [P_{\Omega^\perp} \otimes \Omega \otimes P_{\Omega^\perp} \otimes \Omega]_{:24} + [P_{\Omega^\perp} \otimes \Omega \otimes \Omega \otimes P_{\Omega^\perp}]_{:25} + [\Omega \otimes P_{\Omega^\perp} \otimes \Omega \otimes P_{\Omega^\perp}]_{:35} \right) \end{aligned}$$

$$\begin{aligned} H_4^r(\eta, \Omega, \Omega^\perp) &= \frac{d_{2,4}}{(n-1)(n+1)}T + \frac{d_{4,2}}{n-1} \left(P_{\Omega^\perp} \otimes \Omega \otimes \Omega \otimes \Omega + [P_{\Omega^\perp} \otimes \Omega \otimes P_{\Omega^\perp} \otimes \Omega \otimes \Omega]_{:24} \right. \\ &\quad \left. + [P_{\Omega^\perp} \otimes \Omega \otimes \Omega \otimes P_{\Omega^\perp} \otimes \Omega]_{:25} + [P_{\Omega^\perp} \otimes \Omega \otimes \Omega \otimes \Omega \otimes P_{\Omega^\perp}]_{:26} \right), \end{aligned}$$

Where Γ is symmetric order-4 tensor defined by

$$\Gamma = 3Sym(P_{\Omega^\perp} \otimes P_{\Omega^\perp}). \quad (2.28)$$

In Cartesian coordinates Γ is given by

$$\Gamma_{ijkl} = (P_{\Omega^\perp})_{ij}(P_{\Omega^\perp})_{kl} + (P_{\Omega^\perp})_{ik}(P_{\Omega^\perp})_{jl} + (P_{\Omega^\perp})_{il}(P_{\Omega^\perp})_{jk}.$$

Also, T is a 5-tensor with components

$$T_{ijklp} = \tilde{S}_{ijkl}\Omega_p + \tilde{S}_{ijkp}\Omega_l + \tilde{S}_{ijpl}\Omega_k + \tilde{S}_{ipkl}\Omega_j \quad (2.29)$$

where

$$\tilde{S}_{iii} = 3\Gamma_{iii}, \quad \tilde{S}_{iij} = \Gamma_{iij}, \quad \tilde{S}_{ijj} = \Gamma_{ijj}, \quad \tilde{S}_{jji} = \Gamma_{jji},$$

for $i, j \in \{1, \dots, n\}$ such that $i \neq j$, otherwise \tilde{S}_{ijkl} is zero. Above we used the notation

$$[P_{\Omega^\perp} \otimes \Omega \otimes P_{\Omega^\perp}]_{:24}$$

to denote a 3-tensor whose (i, j, k) component is given by

$$\left([P_{\Omega^\perp} \otimes \Omega \otimes P_{\Omega^\perp}]_{:24}\right)_{ijk} = \sum_{p=1}^n (P_{\Omega^\perp})_{ip} \Omega_j (P_{\Omega^\perp})_{pk},$$

i.e., in this case we contract the full tensor $P_{\Omega^\perp} \otimes \Omega \otimes P_{\Omega^\perp}$, which is a 5-tensor, by summing over the second and the fourth indices (that is why we have the sub-index notation :24). One defines the other contractions analogously.

The proof of the Proposition 2.17 is given in Section 4.4.2.

Moreover, from Theorem 2.16 we can deduce the following:

Corollary 2.18 (Isotropic regime). *Let $n \in \{2, 3\}$ and $a \in (0, 2]$. Suppose that $f^\varepsilon \rightarrow \rho$ as $\varepsilon \rightarrow 0$, then it holds that*

$$\partial_t \rho - D_x \Delta_x \rho + \mu \left(\frac{\chi^2}{n} - 1 \right) \nabla_x \cdot (\rho \nabla_x \rho) = 0. \quad (2.30)$$

Proof. The proof of the corollary directly follows the steps of the proof of Theorem 2.16 to obtain the equation for ρ . \square

The proof of Theorem 2.16 is postponed to Section 4. Next, we comment on Theorem 2.16, particularly on Equations (2.17a) and (2.17b).

2.3 Comments on the continuum equations

In this section we discuss the macroscopic equations for the mass density and the mean-nematic direction (2.17a) and (2.17b), respectively.

2.3.1 The equation for the mass density

Equation (2.17a) is a diffusion-type equation in divergence form and hence the total mass $\int_{\mathbb{R}^n} \rho dx$ is preserved over time. The equation is formed by the sum of a linear diffusion and a non-linear diffusion term. The purely diffusive term with the diffusion constant D_x arises from the Brownian motion at the particle level. The second term on the right-hand-side resembles a porous medium equation, but with a diffusion coefficient K that depends also on the density ρ . Numerical experiments indicate that $K(\eta(\rho))$, as given in Equation (2.18), is non-negative, see Remark 2.19.

Effect of particle anisotropy. Interestingly, the equation for the mass density is independent of the mean-nematic direction Ω . However, the anisotropy of the particles modifies Equation (2.17a). To understand the effect of particle anisotropy, characterised by χ and defined in (1.2), we first consider spherical particles. For spherical particles, $\chi = 0$, and the potential V_b becomes isotropic, i.e.,

$$V_b(x_2 - x_1) = (4\pi)^{-n/2} \exp\left(-\frac{|x_2 - x_1|^2}{2d^2}\right).$$

In this case, particles' positions and directions are completely decoupled in the discrete system (1.3) since $\nabla_u V_b = 0$ and $\nabla_x V_b$ is independent of u . Moreover, one straightforwardly obtains the following equation for ρ (by directly integrating equation (2.4) and noting that $W_f = \rho$ in this case):

$$\partial_t \rho = D_x \Delta_x \rho + \mu \nabla_x \cdot (\rho \nabla_x \rho), \quad \text{for } \chi = 0,$$

which is the porous medium equation with linear diffusion. Notice that it corresponds to Equation (2.30), where we assumed that $f^\varepsilon \rightarrow \rho$ as $\varepsilon \rightarrow 0$. Therefore, the difference between the isotropic and the anisotropic cases is encapsulated in the non-linear diffusion coefficient $K(\eta) \neq 1$.

Now, notice that

$$K(\eta) \leq 1 - \frac{\chi^2}{n},$$

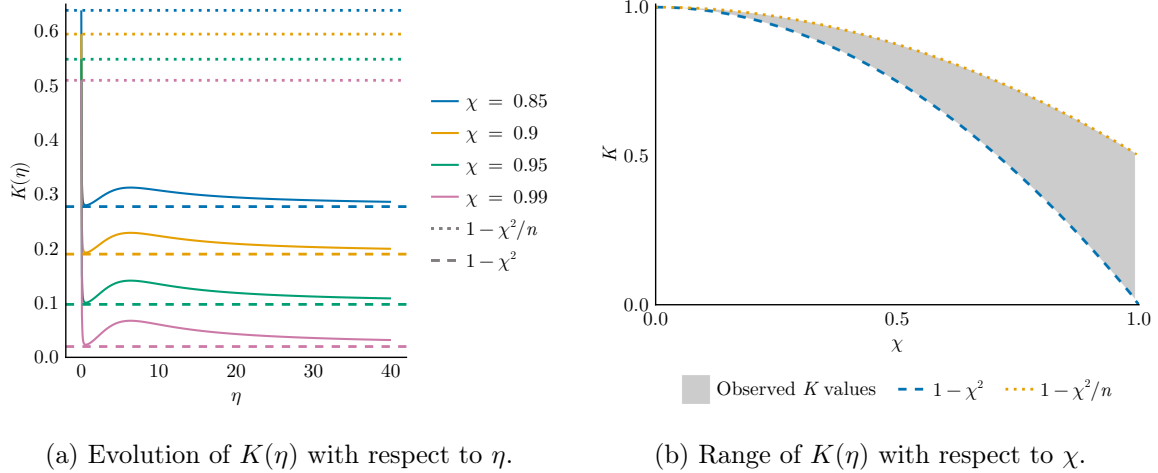
since $S_2(\eta) \in (0, 1)$ and η is non-decreasing (see also Figure 10).

Remark 2.19 (Non-negativity of the diffusion coefficient K). Even though, we do not have an analytical guarantee that K is non-negative, numerical simulations suggest that K actually has a lower bound $1 - \chi^2 \geq 0$. Figure 3a shows the evolution of K as $\eta \geq 0$ varies for different values of χ . The dashed lines in matching colors represent the numerical lower bound for K and the dotted lines display the upper bound $1 - \frac{\chi^2}{n}$ for K . Moreover, in Figure 3b, the gray area shows the range of K values with respect to χ when other parameters, i.e. σ , also vary. Here, we can numerically further confirm that the lower bound for observed K values is $1 - \chi^2$, denoted by the blue dashed line. Note also that, in dimension $n = 3$, χ can take negative values, i.e., $\chi \in [-1, 1]$. However, this does not change the value of K since only χ^2 is involved in the computation of K . That is why we only display $\chi \in [0, 1]$ in Figure 3b and naturally it would be symmetric for $\chi \in [-1, 0]$. Moreover, our numerical experiments include how K changes with respect to ρ for various $\chi \in (0, 1)$ values, see Figure 10c, where, again, K remains non-negative.

Assuming that $K \geq 0$, the particle anisotropy contributes to a slowdown in the non-linear diffusion. In dimension $n = 3$, when the particles are rods ($\chi = 1$) or flat disks ($\chi = -1$) we have that $K(\eta) \leq 2/3$; thus, the original speed of diffusion μ is reduced to at least two-thirds of the anisotropic case. One may hypothesize that this effect is due to anisotropic particles being able to pack and occupy less volume when aligned, so they produce less diffusion. Indeed, our numerical investigations regarding the effect of particle anisotropy on the global alignment also confirm that particles with higher anisotropy reach total global alignment faster. We observe that the particles which are closer to perfect circle in shape ($\chi \approx 0$) and low in density do not reach alignment by the end of the simulation time, whereas particles which are more elongated ellipses ($\chi \approx 1$) with higher densities align globally in a shorter time frame, see, e.g., Figure 7. We refer to Section 3.2.3 for a detailed discussion.

2.3.2 The equation for the mean-nematic direction

First, we remark that the equation for the mean-nematic direction Ω , Equation (2.17b), is non-conservative. It can be verified that $|\Omega|(t)$ remains constant over time, as all the terms lie within the space spanned by Ω^\perp . Consequently, Ω stays on the sphere at all times.



(a) Evolution of $K(\eta)$ with respect to η .

(b) Range of $K(\eta)$ with respect to χ .

Figure 3: (a) Time evolution of the diffusion coefficient $K(\eta)$ with respect to η with different χ values. The dotted lines and the dashed lines correspond to $1 - \chi^2/n$ (upper bound for K) and $1 - \chi^2$ (lower bound for K), respectively, for the matching color χ values. (b) The range of $K(\eta)$ for $\chi \in (0, 1)$ and $\sigma \in [2^{-8}, 2^8]$. The dotted and the dashed lines show the upper and the (numerical) lower bound for K , respectively.

The term Π_2 corresponds to transport of Ω in the direction $\nabla_x \rho$. However, the sign of $\Pi_2(\rho)$ is not immediately clear, or it is uncertain if it changes sign during the dynamics. Notably, Π_2 would vanish if $\mu = 0$, indicating that this term arises from the repulsive potential acting on particle positions.

The last term on the left-hand side of (2.17b) corresponds to diffusion in the direction Ω . The projection term P_{Ω^\perp} ensures that Ω remains on the sphere. One can check that when particles are spherical, there is no equation for Ω , which is expected since the direction Ω does not influence the dynamics in this case. If $\mu = 0$, the diffusion constant reduces to D_x , meaning that, in this case, the diffusion originates only from the Brownian motion of the positions of the particles. Intriguingly, the constant $\mu\sigma$ introduces an anti-diffusion effect.

The case $a \in (0, 2)$. When $a \in (0, 2)$, the right-hand side of (2.17b) vanishes. In this case, the dynamics for ρ and Ω are identical for prolate and oblate particles with the same values of χ^2 . Consequently, at the macroscopic level, the equations do not differentiate between these two types of particles.

2.3.3 The case $a = 2$

When $a = 2$, the term Π_3 , given by Equation (2.21), does not vanish. This term gives the effect of the repulsive potential on the directionality of the particles. Specifically, from Lemma 2.1, the potential V_f^ε expands as

$$V_f^\varepsilon = W_f + \varepsilon^2 B_f + \mathcal{O}(\varepsilon^3),$$

where W_f is a nematic-alignment force, and the term B_f - which generates Π_3 - arises from the specific form of the repulsive potential V_b considered. The term Π_3 involves either second-order differential operators or products of first-order differential operators.

Interpreting Π_3 is not straightforward, but it is clearly distinct from the other terms in Equation (2.17b). Notably, Π_3 is the only term where the distinction between oblate ($\ell < d$) and prolate ($\ell > d$) particles matter. Specifically, oblate and prolate particles exhibit opposite signs for the first and last two terms of Π_3 . If the diffusion constants are positive for prolate particles, they will be negative for

oblate particles, and vice versa. As a result, the qualitative behavior of oblate and prolate particles will differ significantly.

Notice that the second term in Π_3 is solely influenced by the length d . If $d = 0$ (i.e., if the particles are rod-shaped), this term disappears.

To simplify the interpretation of Π_3 , in the next two paragraphs we focus only on dimension $n = 2$.

Anisotropic equilibrium ($d_{2,0} \neq d_{0,2}$). One can expand the contractions in Π_3 further considering expressions (2.22)-(2.25). For example, for the second term in (2.21) we have that:

$$\begin{aligned} [H_2^r : (\Delta_x(\rho H_2))]_{[2,3:1,2]} &= 2d_{2,2}d_{2,0}\Omega^\perp \left(\rho(\Omega^\perp \cdot \Delta_x \Omega) + 2\Omega^\perp \cdot [(\nabla_x \rho \cdot \nabla_x) \Omega] \right) \\ &\quad + 2d_{2,2}d_{0,2}\Omega^\perp \left(\rho(\Omega \cdot \Delta_x \Omega^\perp) + 2\Omega \cdot [(\nabla_x \rho \cdot \nabla_x) \Omega^\perp] \right). \end{aligned}$$

For these equations, it is critical that $d_{2,0} \neq d_{0,2}$, since, if they were the same, then H_2 would be equal to the identity and this would imply that

$$[H_2^r : (\Delta \rho \text{Id})]_{[2,3:1,2]} = 0,$$

since $(\Omega \otimes \Omega^\perp) : \text{Id} = \Omega \cdot \Omega^\perp = 0$. Moreover, if $d_{2,0} = d_{0,2}$, then the third term of (2.21) would become:

$$[H_4^r : D_x^2 \otimes \rho \text{Id}]_{[2,3,4,5:1,2,3,4]} = d_{2,0}(d_{2,4} + d_{4,2})\Omega^\perp [(\Omega \otimes \Omega^\perp + \Omega^\perp \otimes \Omega) : (D_x^2 \rho)].$$

Therefore, the fact that $d_{2,0} \neq d_{0,2}$ creates an anisotropy that produces derivatives in Ω and Ω^\perp . If $G_{\eta(\rho)A_\Omega}$ was the uniform distribution (i.e., if $\ell = d$), then we would have that $d_{2,0} = d_{0,2}$. Thus, this effect is linked to the anisotropy of the particles.

Cross-diffusion term. The term of Π_3 containing the second derivatives of ρ is

$$b(\rho)\rho\Omega^\perp [(\Omega \otimes \Omega^\perp + \Omega^\perp \otimes \Omega) : D_x^2 \rho],$$

where

$$b(\rho) := \frac{n-1}{8\eta(\rho)c_{1,2}} (\ell^2 - d^2) (d_{2,2} - \chi^2(d_{4,2}d_{2,0} + d_{2,4}d_{0,2}) - 2\chi^2 d_{2,2}^2).$$

This term makes the system (2.17a)-(2.17b) of a cross-diffusion type. In dimension $n = 3$, it is clear that if the diffusion coefficient $b(\rho)$ is positive for prolate particles then it is negative for oblate particles (and vice versa). This will particularly complicate the study of the well-posedness of the equations, which we leave for future work.

2.4 Parameter regime for the validity of the continuum equations

It remains an open question to determine for which parameter regime the macroscopic equations (2.17a)-(2.17b) are well-posed. In particular, the consistency relation (2.14) imposes a major constraint on the dynamics. Particularly, when $\rho < \rho_*$, the macroscopic equations lose their validity. In this section, we illustrate this effect with a couple of examples.

Diffusion term in Ω . For the well-posedness of the equations, we require the diffusion constant in Ω , given by $\mu(\nu - \sigma)$, (see the left-hand side of (2.17b)), to be positive. This is equivalent to the condition:

$$\frac{\mu}{D_x} < \frac{\lambda}{D_u}.$$

This condition establishes a balance between the noise intensities D_x, D_u and the intensity of the alignment interactions μ, λ . If $\mu = \lambda$, then we must have $D_u < D_x$ (i.e., the noise intensity in the directions must be smaller than in the positions). If $D_x = D_u$, then $\mu < \lambda$ must hold (i.e., the intensity of the potential must be stronger for the directions than for the positions). Additionally, for well-posedness, it is required that $D_x > 0$. These parameter constraints suggest that there are certain aspects of the microscopic dynamics that the macroscopic equations fail to capture. Moreover, in Section 3.2, we present some numerical tests on this condition at the microscopic level, simulating the stochastic particle system (1.3). The results indicate that when the continuum equations are ill-posed, i.e., when $\sigma \geq \nu$, the particles do not reach any type of alignment. This can be observed particularly in Figures 4 and 5. For further details, we refer the reader to Section 3.2.

The critical case $\nu = \sigma$. Let us consider the critical case where $\nu = \sigma$. In this case the diffusive term in Ω vanishes. We explore this scenario in more detail.

Notice that we can rewrite the kinetic equation (2.6) (for $a \in (0, 2)$) as:

$$\begin{aligned} \partial_t f^\varepsilon - D_x \nabla_x \cdot \left(\nabla_x f^\varepsilon - \frac{\chi^2 \mu}{D_x} f^\varepsilon \nabla_x (u^T (\rho_f Q_f) u) \right) + \mu \left(\frac{\chi^2}{n} - 1 \right) \nabla_x \cdot ((\nabla_x \rho_{f^\varepsilon}) f^\varepsilon) \\ = \frac{D_u}{\varepsilon} C(f^\varepsilon) + \mathcal{O}(\varepsilon^2), \end{aligned} \quad (2.31)$$

where, we recall,

$$C(f) = \nabla_u \cdot \left(\nabla_u f - \frac{\chi^2 \lambda}{D_u} f \nabla_u (u^T (\rho_f Q_f) u) \right).$$

Notice that the second term in (2.31) has the same shape as the operator C except that the derivatives are in x and the parameter values differ.

If $\nu = \sigma$, i.e., $\frac{D_x}{\mu} = \frac{D_u}{\lambda}$, the second term in (2.31) can be rewritten as

$$-D_x \nabla_x \cdot \left(G_{\alpha \rho_f Q_f} \nabla_x \left(\frac{f^\varepsilon}{G_{\alpha \rho_f Q_f}} \right) \right), \quad \text{with } \alpha = \frac{\chi^2}{\sigma}. \quad (2.32)$$

By Lemma 2.10, when $f^\varepsilon \rightarrow \rho G_{\eta(\rho)A\Omega}$, we have that $G_{\alpha \rho_f Q_f} \rightarrow G_{\eta(\rho)A\Omega}$ and in the limit (2.32) becomes

$$-D_x \nabla_x \cdot (G_{\eta(\rho)A\Omega} \nabla_x \rho).$$

Integrating (2.31), and using the fact that $\int G_{\eta(\rho)A\Omega} du = 1$, we obtain Equation (2.30), which is the equation obtained in the isotropic regime corresponding to $f^\varepsilon \rightarrow \rho$ as $\varepsilon \rightarrow 0$. A possible explanation for this is that when $\mu = \sigma$ the density ρ declines rapidly below the critical density ρ_* due to the diffusive processes involved.

In conclusion, we emphasize two main takeaways on the validity of the continuum equations. Firstly, the macroscopic limit does not hold for arbitrary parameter values. Secondly, the macroscopic equation ceases to be valid when $\rho < \rho_*$ (at the points where Equation (2.30) holds and we enter the isotropic regime). However, we have no prior information on the specific points in space or the times at which this may occur.

We finish with a remark concerning the validity of the continuum equations for higher dimensions.

Remark 2.20 (Higher dimensions). The macroscopic limit presented in this paper only holds for $n \in \{2, 3\}$ since in Lemma 2.10 we only obtain stable equilibria for these dimensions. Existence of stable equilibria for $n \geq 4$ is an open problem. However, if Lemma 2.10 holds for $n \geq 4$, we could conjecture that Theorem 2.16 would also hold for $n \geq 4$.

3 Repulsive potentials and particle simulations

In this section, we comment on the different Gaussian-type repulsive potentials, motivate our choice (1.6) and present numerical simulations for particles following the dynamics (1.3a)-(1.3b).

3.1 Gaussian-type anisotropic repulsive potentials

Earlier, we described the binary interactions between identical particles via an anisotropic potential V_b given by Equation (1.4). We comment on two particular choices of the scaling factor $b \geq 0$ in (1.4).

The Berne-Pechukas potential. One of the first soft anisotropic potentials that appeared in the literature is that of a soft repulsive potential between two spheroids using the Gaussian potential. It was first introduced by Berne and Pechukas in [5]. In [5], the scaling factor $b(u_1, u_2)$ is given by

$$b_{\text{BP}}(u_1, u_2) := (1 - \chi^2(u_1 \cdot u_2)^2)^{-1/2} = \det(\Sigma)^{-1/2}, \quad (3.1)$$

where χ is defined by (1.2). This is a very natural choice for the scaling factor b , as it guarantees that V_b is a multivariate Gaussian distribution in the variable R with a covariance matrix given by $\Sigma/2$.

The non-scaled Gaussian potential. Berne and Pechukas in [5] considered a scaling factor b such that the potential (1.4) is normalized, i.e., $\int_{\mathbb{R}^d} V_{b_{\text{BP}}}(u_1, u_2, R) \, dR = 1$. However, one could choose to work directly with the potential without normalization, i.e., consider the scaling factor

$$b_{\text{NR}}(u_1, u_2) := (4\pi)^{n/2}. \quad (3.2)$$

Notice that both, the potential $V_{b_{\text{BP}}}$ and the potential without normalization $V_{b_{\text{NR}}}$, have the same level sets in space (up to scaling). The level sets in directions, however, are different and this has important consequences.

3.1.1 Motivation for the interaction potential

We focus on the non-scaled Gaussian potential for two reasons. Firstly, the Berne-Pechukas potential does not produce nematic alignment at first order, see below item (ii). Secondly, we want to avoid the modification in the directions introduced by the scaling. However, considering a system interacting via this potential is mathematically challenging to study, and, therefore, we consider a modified version of the non-scaled Gaussian potential, retaining the similar properties, this was explained in Remark 1.1. Instead of (3.2), we work with (1.6), as introduced earlier. This simplification resembles to the simplification done when considering the Maier-Saupe potential $b_{\text{MS}}(u, u') := (u \cdot u')^2$ instead of the Onsager potential $b_{\text{O}}(u, u') := |u \cdot u'|$, see, [31]. Both potentials have the same minimizer, but b_{MS} is easier to study mathematically.

Moreover, using (1.6), we then observe that the leading term of the expansion (2.1) is given by

$$W_f(t, x_1, u_1) := \int_{\mathbb{S}^{n-1}} (1 - \chi^2(u_1 \cdot u_2)^2) f(t, x_1, u_2) \, du_2.$$

The function inside the integrand $\varphi(u_1, u_2) := (1 - \chi^2(u_1 \cdot u_2)^2)$ resembles that of the Maier-Saupe potential [31] and motivates our choice for the rescaling factor b . In particular,

(i). if we consider $b \equiv 1$ (i.e., without scaling of the potential), we obtain

$$\tilde{W}_f(t, x_1, u_1) := \int_{\mathbb{S}^{n-1}} (1 - \chi^2(u_1 \cdot u_2)^2)^{1/2} f(t, x_1, u_2) du_2,$$

with $\tilde{\varphi}(u_1, u_2) := (1 - \chi^2(u_1 \cdot u_2)^2)^{1/2}$. Even though the potential with φ and the potential with $\tilde{\varphi}$ have the same minimizers in terms of u_1, u_2 , W_f is more straightforward to analyze since we can rewrite it as

$$W_f(t, x_1, u_1) = u_1^T \left(\int_{\mathbb{S}^{n-1}} (\text{Id} - \chi^2(u_2 \otimes u_2)) f(t, x_1, u_2) du_2 \right) u_1,$$

i.e., we can decouple the variables u_1 and u_2 and recast W_f in terms of Q_f (see Equations (1.9) and (2.5)). As previously mentioned, a similar simplification is done when, instead of considering the Onsager potential $b_O(u_1, u_2) = |u_1 \cdot u_2|$, one considers the Maier-Saupe potential $b_{MS}(u_1, u_2) = (u_1 \cdot u_2)^2$, see [31] for more details.

(ii). If we consider the Berne-Pechukas scaling b_{BP} in (3.1), then the corresponding potential takes the form

$$W_f^{BP}(t, x_1) = \int_{\mathbb{S}^{n-1}} f(t, x_1, u_2) du_2 = \rho(t, x_1). \quad (3.3)$$

Since the total integral of $V_{b_{BP}}$ is one, we do not obtain a nematic alignment potential at the leading order.

In Section 3.2.4, we provide a numerical comparison of stochastic particle systems interacting via these different potentials. Indeed, we observe that particles interacting via the Berne-Pechukas potential do not align, see Figure 9.

3.2 Numerical simulations

This section is dedicated to the numerical simulations of the stochastic particle system (1.3), particularly to compare the particle-level dynamics at longer times with our analytical predictions on the macroscopic dynamics.

We start with the study of how the central assumption for well-posedness (1.10) at the macroscopic level affects the particle dynamics. Subsequently, we investigate the impact of the anisotropy of the particles (measured by χ defined in (1.2)) and the particle density on the particle interaction dynamics. We finish the numerical simulations section with a comparison between the different types of interaction potentials mentioned in Section 3.1.

The source code for the particle simulations is provided at

https://github.com/cwytrzens/anisotropic_particles.

3.2.1 Numerical implementation

We simulate the discrete particle dynamics in dimension $n = 2$, governed by the stochastic differential equations (1.3a) and (1.3b) on a periodic domain. The simulations use an explicit Runge-Kutta Milstein method of strong order 1 with adaptive time stepping. This numerical method is part of the Julia package `StochasticDiffEq.jl`, see [27]. Since we want to study a wide range of model parameters, it is crucial to use an adaptive time-stepping method, as the stiffness of the system strongly depends on the model parameters and differs across the parameter range that we investigate. We use default tolerance parameters `reltol` = 10^{-2} and `abstol` = 10^{-2} . Moreover, in order to allow faster numerical

evaluations of the interaction forces, we truncate the potential V_b as defined in Equation (1.4) for $R = |X_j - X_i| \geq 8 \max(\ell, d)$.

For the particle simulations, we consider a square domain of size $[0, L_x] \times [0, L_y]$ with $L_x = L_y = 100$ and fix the number of particles at $N = 10^5$. The initial positions X_i and directions u_i of the particles are taken uniform and random for $i = 1, \dots, N$. Moreover, we set $t_{\text{end}} = 1.5 \times 10^5$, the time at which the simulations stop.

We perform an extensive parameter study for each remaining parameter pair, namely, the diffusion constants in space D_x and direction D_u ; the strength factors of the repulsive force, μ and λ ; the anisotropy parameter χ , and the particle density $\bar{\rho}$ which we define as

$$\bar{\rho} := \frac{\pi \ell d N}{L_x L_y}, \quad (3.4)$$

and it represents the ratio of the total volume of all particles to the domain size. The parameters χ and $\bar{\rho}$ determine d and ℓ uniquely (by solving (1.2) and (3.4) for d and ℓ).

3.2.2 Parameter study

For the parameter study, we focus on capturing the regime of parameter values at which the global alignment is reached versus those at which the particles fail to align globally. As the dynamics depend on many parameters and the balance between them, capturing all interesting parameter combinations is very challenging; thus, out of the scope of this numerical study. To measure alignment, we compute the order parameter γ_f which is given in (2.16). If not stated otherwise, all the simulations use the default parameters given in Table 1.

Parameter	Value
χ	0.9
$\bar{\rho}$	1
D_x	2^{-4}
D_u	2^{-11}
λ	2^8
μ	2^{13}
N	10^5
L_x, L_y	100
t_{end}	1.5×10^5

Table 1: Default model parameters for the simulations of the particle system.

To capture the transition to alignment, we typically vary one or two parameters while keeping the others fixed. This approach allows for a direct comparison between our numerical results and the theoretical prediction that the condition $\sigma < \nu$ is necessary for well-posedness of the continuum equations, see (1.10). Recalling that $\sigma = \frac{D_u}{\lambda}$ and $\nu = \frac{D_x}{\mu}$, we study the trajectories of the order parameter γ_f by varying D_u relative to D_x , and λ relative to μ , while keeping the remaining parameters constant.

Another primary feature of our particle system is the global alignment induced by the anisotropy of the particles. To investigate this feature, we conduct a parameter study of χ versus $\bar{\rho}$. Specifically, we study the impact of the anisotropy parameter χ on global alignment by defining the parameters ℓ and d implicitly in terms of χ and $\bar{\rho}$.

For each parameter pair (D_x, D_u) , (λ, μ) , and $(\chi, \bar{\rho})$, we present three plots:

- (a) The expected trajectories of the mean global alignment γ_f , obtained by varying one parameter while keeping the others constant.
- (b) A similar plot for the second parameter of the pair.
- (c) A heatmap of the mean order parameter γ_f at the final simulation time t_{end} , obtained by varying both parameters simultaneously. The heatmap highlights the transition to alignment with the transition front ($\sigma = \nu$) marked by a red line.

For each parameter combination, we collect 8 simulation samples to estimate the trajectory of the mean global alignment, where the matching color bands show the standard deviation.

3.2.3 Simulation results

In this section, we present the results of our numerical experiments.

We start with the study of our first parameter pair, diffusion constants D_x and D_u , presented in Figure 4. Figure 4a displays the trajectories of the order parameter γ_f over time for different values of $D_x = 2^{-k}$ for $k = 2, \dots, 7$ and D_u fixed at 0. Hence, there is no noise present in the particle directions u . We observe that the smaller the value of D_x , the slower the emergence of the global alignment. We fix $D_x = 2^{-4}$ as the default value and look at various D_u values in Figure 4b.

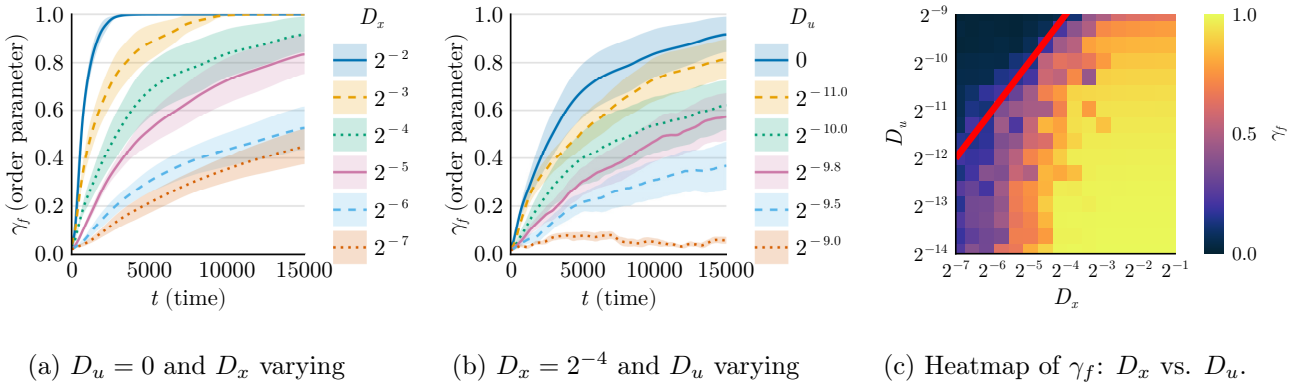


Figure 4: Parameter study for (D_x, D_u) . Trajectories of the order parameter γ_f are plotted for fixed $D_u = 0$ and varying D_x in Figure 4a; for fixed $D_x = 2^{-4}$ and varying D_u in Figure 4b. Figure 4c displays a heatmap of γ_f at time $t_{\text{end}} = 1.5 \times 10^5$ while both D_u and D_x vary simultaneously. The red line depicts where $\nu = \sigma$.

We observe an opposite effect for D_u . In Figure 4b, varying D_u shows that less angular noise leads to quicker alignment and too large noise might prevent reaching alignment all-together.

Finally, in Figure 4c, we display the order parameter γ_f at the final simulation time t_{end} as a heatmap of varying D_x versus D_u . Here, we observe the parameter range leading to alignment and a transition along level sets of D_x versus D_u . At the particle level, the heatmap can be interpreted as follows. Increasing the positional noise facilitates interactions among a greater variety of particles, as neighboring particles change quickly, which contributes to reaching global alignment. On the contrary, increasing the directional noise drives the system away from global alignment, which is, in particular, critical if particles only interact with their nearest neighbors. Consequently, we observe a lack of alignment in the top left corner of the heatmap, where positional noise is low and directional noise is high.

Note that the red line displays where $\nu = \frac{D_x}{\mu} = \frac{D_u}{\lambda} = \sigma$. This indicates the interface at which the macroscopic equation (2.17b) for the mean-nematic direction Ω_f becomes ill-posed, see the discussion

on well-posedness in Section 2.4. Crucially, the right-hand side of this red line is the parameter regime ($\sigma < \nu$) where the macroscopic equations remain well-posed, and it is exactly in this parameter regime that we observe the onset of particle alignment.

In Figure 5, we investigate how the forces acting on positions X_i and directions u_i affect the alignment of particles. The strength factors of these forces are determined by the positive constants μ and λ in front of the interaction terms in Equations (1.3a) and (1.3b).

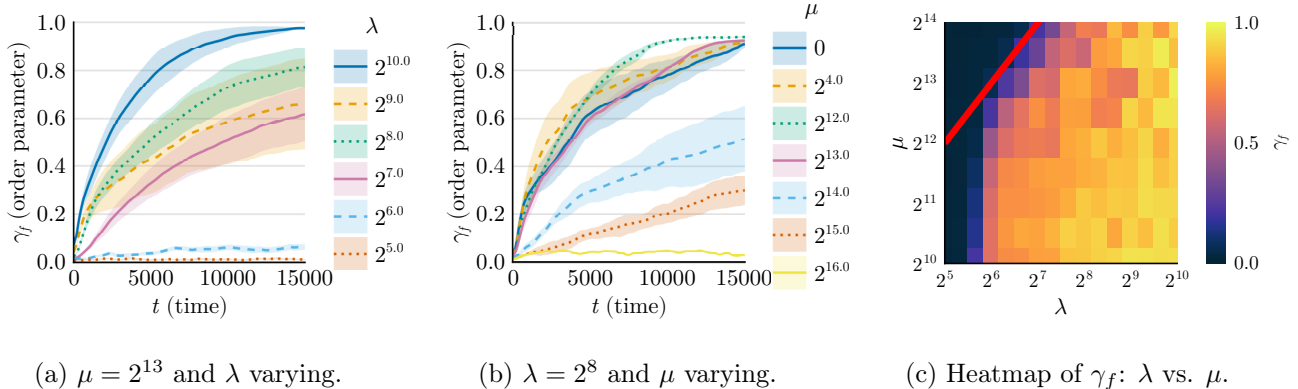


Figure 5: Parameter study for (λ, μ) . Trajectories of the order parameter γ_f are plotted for fixed $\mu = 2^{13}$ and varying λ in Figure 5a; for $\lambda = 2^8$ and varying μ in Figure 6a. Figure 5c displays the heatmap of γ_f at time $t_{\text{end}} = 1.5 \times 10^5$ while both λ and μ vary simultaneously. The red line depicts where $\nu = \sigma$.

Figure 5a shows the trajectories of the order parameter γ_f over time for fixed $\mu = 2^{13}$ and varying values of λ from 2^5 to 2^{10} . We observe that for $\lambda \leq 2^6$, the system is in total chaos, with γ_f close to 0, indicating that the force acting on the particles' directions is not strong enough to drive the system towards alignment. Additionally, we deduce that as λ increases, γ_f appears to increase accordingly.

Next, we fix $\lambda = 2^8$ and vary μ from 0 to 2^{16} to study how the strength of the potential V_b affects the alignment through the force acting on the particles' positions. In Figure 5b, we observe that μ must be sufficiently large to have a significant impact on the particle dynamics. As μ increases, the particles lose their alignment, see, e.g., when $\mu = 2^{16}$, γ_f is very close to 0.

Lastly, we present a heatmap of the order parameter γ_f in Figure 5c, similar to Figure 4c, but for λ versus μ . Similarly, the red line displays the interface of the analytical well-posedness condition $\nu = \sigma$, see Equation (1.10). Again, we observe that global alignment only occurs inside the parameter range where the macroscopic equations are well-posed ($\sigma < \nu$), located on the right-hand side of the red line.

As for our last parameter pair, in Figure 6 we study the effects of the anisotropy χ and the density of particles $\bar{\rho}$ on the global alignment. In Figure 6a, we present a plot of the trajectories of γ_f when $\bar{\rho} = 1$ and the anisotropy parameter χ is varying from 0.6 to 1. We can clearly deduce that a certain degree of anisotropy is required for particles to reach global alignment.

In Figure 6b, we fix $\chi = 0.9$ and vary $\bar{\rho}$ from 0.5 to 2 (recall that $\bar{\rho}$ is computed using (3.4)) and plot the trajectories of γ_f . We observe that the particle density must also be sufficiently high for particles to align, otherwise, if the particles are too far apart, the repulsive potential is not strong enough to induce alignment. Figure 6c presents a heatmap illustrating the effect of both χ and $\bar{\rho}$ on the transition towards a higher-order alignment. Here, we also observe a clear linear progression, moving from a chaotic state, where γ_f is close to 0, to a well-ordered system, characterized by global alignment with $\gamma_f \approx 1$.

Moreover, to further investigate the effect of the shape of the particles on the global alignment of the system, we present in Figure 7 another heatmap of γ_f with the same dataset as in Figure 6c. However, in Figure 7 we compare the effect of varying the lengths of the major and the minor axes of the ellipses,

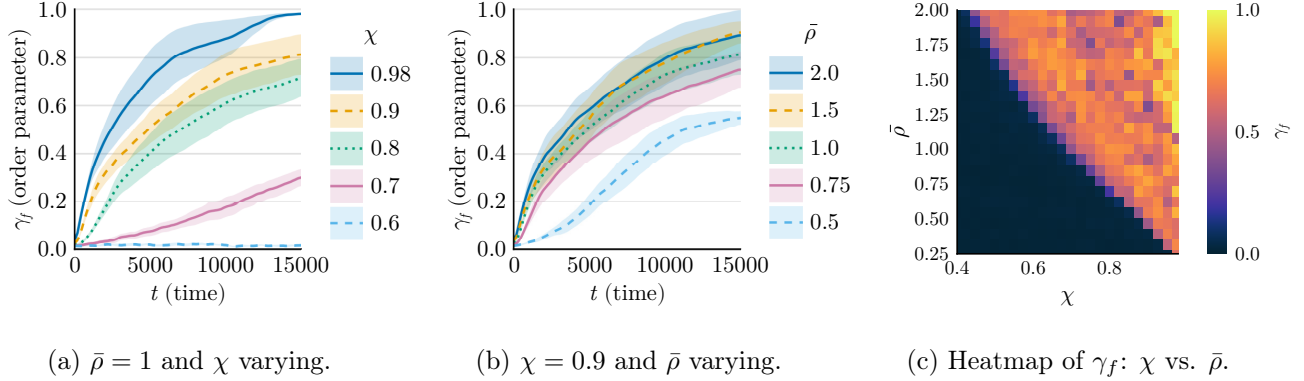


Figure 6: Parameter study for $(\chi, \bar{\rho})$. Trajectories of the order parameter γ_f are plotted for fixed $\bar{\rho} = 1$ and varying χ in Figure 6a; for fixed $\chi = 0.9$ and varying $\bar{\rho}$ in Figure 6b. Figure 6 displays the heatmap of γ_f at time $t_{\text{end}} = 1.5 \times 10^5$ while both χ and $\bar{\rho}$ vary simultaneously.

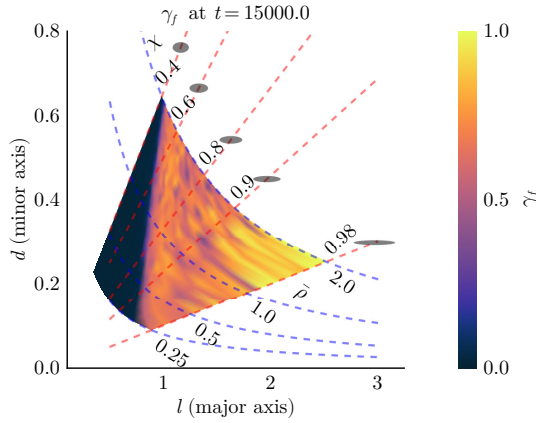


Figure 7: Heatmap of γ_f : χ versus $\bar{\rho}$. The dashed red lines display the anisotropy parameter χ for the corresponding lengths of the major and minor axes of the ellipses, ℓ and d respectively. Ellipses with corresponding χ are pictured in gray. The dashed blue lines are the constant density curves $\bar{\rho}$ corresponding to ℓ and d , computed using (3.4).

i.e., ℓ and d , on global alignment rather than with respect to χ and $\bar{\rho}$. Notice that depending on ℓ and d , both χ and $\bar{\rho}$ vary across the heatmap accordingly. The red dashed lines display the constant χ curves, and similarly the blue dashed lines represent the constant $\bar{\rho}$ curves. This figure also confirms that the larger the particle anisotropy, the easier global alignment is achieved.

We remark that these numerical findings are in total agreement with our analytical conclusions. More precisely, at the macroscopic level, this behavior is also evident since the repulsive potential V_b ultimately gives rise to the nematic alignment potential with the factor $1 - \chi^2(u \cdot u_2)^2$ in Equation (2.2). Consequently, when particles are circular ($\chi = 0$), no alignment is observed at the macroscopic level. Also the effect of the potential is less for smaller values of χ .

We end this section with several snapshots of a particle simulation. In Figure 8, we start with a completely random state on the upper left figure and run the simulation using the default parameters in Table 1. Above each snapshot, we display the time at which the snapshot was captured with together with the value of the order parameter γ_f of the system at that time. The colors represent the nematic direction of the particles.

The particles start to align over time and hence, the also the order parameter γ_f increases in time. Finally, the bottom right snapshot in Figure 8 shows that the system reaches a globally aligned state with $\gamma_f = 0.92$, displayed in uniform colors, at the final simulation time t_{end} .

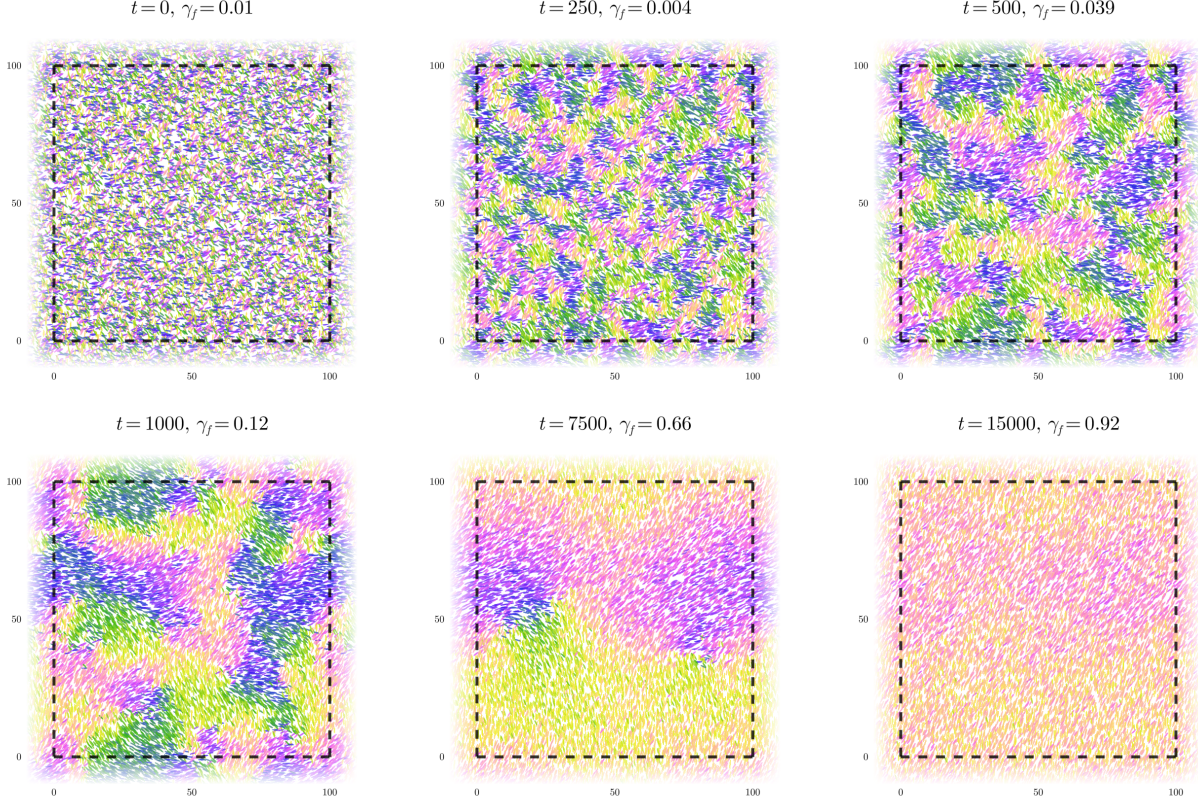


Figure 8: Snapshots of a particle simulation at different times using the default parameters given in Table 1. Different colors represent the different nematic directions of the particles. For the corresponding movie and movies for other cases see link <https://doi.org/10.6084/m9.figshare.27117136.v1>.

3.2.4 Numerical comparison of the potentials

Another prediction we draw from our mathematical analysis in Section 3.1 is the lack of alignment in the case of the Berne-Pechukas potential (3.3). To test this hypothesis numerically, we consider an interpolation between the weighted Gaussian potential and the Berne-Pechukas potential,

$$V_\xi(u_1, u_2, R) := (4\pi)^{-n/2} \det(\Sigma)^{\frac{1}{2}-\xi} \exp(-R^T \Sigma^{-1} R),$$

where $\xi \in [0, 1]$ and recalling that $\det(\Sigma) = 1 - \chi^2(u_1 \cdot u_2)^2$. Notice that V_ξ corresponds to

- the weighted Gaussian potential, given by $V_{b_{\text{WG}}}$ (1.6), when $\xi = 0$,
- the non-scaled Gaussian potential $V_{b_{\text{NR}}}$, obtained by using the scaling factor (3.2), when $\xi = \frac{1}{2}$,
- the Berne-Pechukas potential $V_{b_{\text{BP}}}$, obtained by using the scaling factor (3.3), when $\xi = 1$.

We remark that with increasing ξ , the scale of the potential might change, since we have

$$\frac{V_\xi}{V_{b_{\text{WG}}}} = \frac{(1 - \chi^2(u_1 \cdot u_2)^2)^{\frac{1}{2}-\xi}}{(1 - \chi^2(u_1 \cdot u_2)^2)^{\frac{1}{2}}} \leq \frac{1}{(1 - \chi^2)^\xi}.$$

In Section 3.2.3, we observed (see Figure 5) that increasing λ increases the order parameter γ_f ; thus, has a positive effect on the global alignment. Therefore, we consider the scaling $\lambda = ((1 - \chi^2)^{2\xi})\lambda'$ so

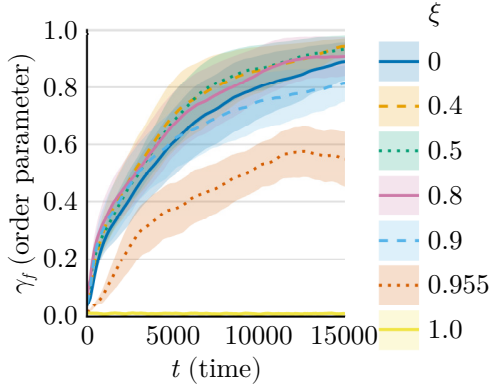


Figure 9: Trajectories of the order parameter γ_f are plotted for varying ξ and the remaining parameters are fixed at their default values given in Table 1. For $\xi = 0$, $\xi = 1/2$ and $\xi = 1$, V_ξ corresponds to the weighted Gaussian potential $V_{b_{\text{WG}}}$, the non-scaled Gaussian potential $V_{b_{\text{NR}}}$ and the Berne-Pechukas potential $V_{b_{\text{BP}}}$, respectively.

that increasing ξ increases λ' and speeds up the alignment. Notice that here we chose the exponent 2ξ instead of just ξ to promote even stronger alignment for larger ξ values. For the simulations we use the default parameters listed in Table 1.

Figure 9 displays the trajectories of the order parameter γ_f for different values of ξ . We clearly observe a sharp transition from higher ordered states to a disordered state (where γ_f is nearly 0) as we increase $\xi = 0$ (the weighted Gaussian potential) to $\xi = 1$ (the Berne-Pechukas potential). Moreover, we also obtain global alignment for $\xi = \frac{1}{2}$ (the non-scaled Gaussian potential). Thus, our numerical study of the potentials strongly supports our analytical predictions in Section 3.1.

Summary of the numerical studies. In this section, we conducted comprehensive numerical parameter studies on various parameter pairs: (D_x, D_u) , (λ, μ) , and $(\chi, \bar{\rho})$. We also compared different interaction potentials by simulating the stochastic particle system (1.3). Given the complex dynamics governed by (1.3), it is numerically very challenging to determine all the interesting parameter regimes. Hence, we focused on the transitional ranges where global alignment breaks down. While the observed trends can be intuitively explained at the particle level, they are closely linked to our analytical results in the following ways:

- Global alignment fails to emerge for parameters where the macroscopic equation for the mean-nematic alignment Ω is ill-posed, as characterized by the well-posedness condition (1.10). This effect is evident in Figures 4c and 5c.
- Particle shape and density significantly influence the phase transition towards global alignment. As predicted by the macroscopic equations, spherical particles and low densities result in slower rates of alignment or a complete lack thereof.
- Our numerical tests confirm that the Berne-Pechukas potential does not lead to global alignment at the particle level, which aligns with the macroscopic perspective presented in Section 3.1.

4 Proof of Theorem 2.16

This section is dedicated to the proof of our main result, Theorem 2.16. First we give some preliminary tools that will be used later in the proof.

4.1 Preliminaries

Change of variables. In the sequel, we apply repeatedly the following change of variables $u \mapsto (\theta, v)$ where $u \in \mathbb{S}^{n-1} \setminus \{\pm\Omega\}$ and $(\theta, v) \in (0, \pi) \times \mathbb{S}^{n-2}$ defined by

$$\begin{aligned} u &= (u \cdot \Omega)\Omega + P_{\Omega^\perp}(u) = \cos \theta \Omega + \sin \theta v, \\ du &= \sin^{n-2} \theta \, d\theta \, dv, \end{aligned} \quad (4.1)$$

where \mathbb{S}^{n-2} is identified as $\mathbb{S}^{n-1} \cap \Omega^\perp$. For simplicity, we assume that the measure du is such that the total mass of the sphere is 1, i.e., $\int_{\mathbb{S}^{n-1}} du = 1$. In the course of the proof, we will also apply this change of variables to the Gibbs distribution $G_{\eta(\rho)A\Omega}$ as stated in (2.10). Hence, we define

$$g_\eta(\theta) := \frac{e^{\eta(\rho) \cos^2 \theta}}{Z_\eta}, \quad \text{where} \quad Z_\eta = \int_0^\pi e^{\eta(\rho) \cos^2 \theta'} \, d\theta'. \quad (4.2)$$

as the transformed Gibbs distribution. Indeed, notice that the value of the normalizing factor Z_η does not depend on Ω , but it depends on $\eta = \eta(\rho)$. For more details on this change of variables see [19].

Derivatives and integrals. Since we will use various derivatives of $G_{\eta(\rho)A\Omega}$, we collect them below in the following Lemma:

Lemma 4.1. *Let $G_{\eta(\rho)A\Omega}$ be the Gibbs distribution defined in (2.10). Then the following holds,*

$$\begin{aligned} \frac{\partial G_{\eta(\rho)A\Omega}}{G_{\eta(\rho)A\Omega}} &= \eta'(\rho)(\partial\rho) \left((u \cdot \Omega)^2 - d_{2,0}(\rho) \right) + 2\eta(\rho)(u \cdot \Omega)(u \cdot \partial\Omega), \\ \frac{\nabla_x G_{\eta(\rho)A\Omega}}{G_{\eta(\rho)A\Omega}} &= \eta'(\rho)(\nabla_x \rho) \left((u \cdot \Omega)^2 - d_{2,0}(\rho) \right) + 2\eta(\rho)(u \cdot \Omega)(u \cdot \nabla_x \Omega), \\ \frac{\partial^2 G_{\eta(\rho)A\Omega}}{G_{\eta(\rho)A\Omega}} &= \partial^2 \eta \left((u \cdot \Omega)^2 - d_{2,0}(\rho) \right) + \partial\eta \left(4(u \cdot \Omega)(u \cdot \partial\Omega) - \partial d_{2,0}(\rho) \right) \\ &\quad + 2\eta(u \cdot \partial\Omega)^2 + 2\eta(u \cdot \Omega)(u \cdot \partial^2 \Omega) + \left(\partial\eta \left((u \cdot \Omega)^2 - d_{2,0}(\rho) \right) + 2\eta(u \cdot \Omega)(u \cdot \partial\Omega) \right)^2, \end{aligned} \quad (4.3)$$

where ∂ denotes the partial derivative with respect to time or with respect to one of the spatial components, i.e., $\partial = \partial_t$, or $\partial = \partial_{x_i}$, $i = 1, \dots, n$; $\nabla_x \Omega$ is a matrix such that $(\nabla_x \Omega)_{ij} = \partial_{x_j} \Omega_i$ and thus $(u \cdot \nabla_x \Omega)_i = u \cdot \partial_{x_i} \Omega$ and $(\partial^2 \Omega)_i = \partial^2 \Omega_i$.

Proof. The proof follows directly from straightforward computations. \square

Lemma 4.2. *Let h_η be any odd function, $w \in \mathbb{R}^n$, and $k \in \mathbb{N} \cup 0$. Then the following holds for $\psi(u) := h_\eta(u \cdot \Omega) P_{\Omega^\perp} u$:*

$$\int_{\mathbb{S}^{n-1}} (u \cdot \Omega)^k G_{\eta(\rho)A\Omega} \psi(u) \, du = 0, \quad (4.4)$$

$$\int_{\mathbb{S}^{n-1}} (u \cdot w)(u \cdot \Omega)^k G_{\eta(\rho)A\Omega} \psi(u) \, du = \frac{c_{k,2}}{n-1} P_{\Omega^\perp} w, \quad (4.5)$$

$$\int_{\mathbb{S}^{n-1}} (u \cdot \Omega)^k \partial G_{\eta(\rho)A\Omega} \psi(u) \, du = \eta(\rho) \frac{2c_{k+1,2}}{n-1} \partial\Omega, \quad (4.6)$$

$$\int_{\mathbb{S}^{n-1}} (u \cdot w)(u \cdot \Omega)^k \partial G_{\eta(\rho)A\Omega} \psi(u) \, du = \eta'(\rho)(\partial\rho)(c_{k+2,2} - d_{2,0}c_{k,2}) \frac{1}{n-1} w \quad \text{for } w \perp \Omega, \quad (4.7)$$

$$\int_{\mathbb{S}^{n-1}} (u \cdot \Omega)^{2k} (u \cdot w)^2 G_{\eta(\rho)A\Omega} \psi(u) \, du = 0 \quad \text{for } w \perp \Omega, \quad (4.8)$$

$$\int_{\mathbb{S}^{n-1}} \partial^2 G_{\eta(\rho)A\Omega} \psi(u) \, du = \frac{4}{n-1} (c_{1,2} + \eta(\rho)(c_{3,2} - d_{2,0}c_{1,2})) \partial\eta \partial\Omega + \frac{2c_{1,2}}{n-1} \eta(\rho) P_{\Omega^\perp} \partial^2 \Omega, \quad (4.9)$$

where the partial derivatives are with respect to time or space, i.e., $\partial = \partial_t, \partial_{x_i}$ with x_i being the i -th component of x and the coefficients $c_{k,p}, d_{k,p}$ are given in (2.19) and (2.20). Moreover, it also holds that

$$d_{k,p} = 0 \quad \text{for } k \text{ odd} \quad \text{and} \quad c_{k,p} = 0 \quad \text{for } k \text{ even.}$$

Proof. The proof of this lemma can be found in Appendix A.2. □

Finally, notice that

$$\partial\Omega \perp \Omega$$

for $\partial = \partial_t, \partial_{x_i}$ (since $\Omega \cdot \partial\Omega = \partial|\Omega|^2/2 = 0$). Therefore, it holds that

$$P_{\Omega^\perp} \partial\Omega = \partial\Omega. \tag{4.10}$$

Next, we consider the following integrals with respect to $v \in \mathbb{S}^{n-2}$.

Lemma 4.3 (Lemma 4.1 in [19]). *Let $n \geq 2$ and $v \in \mathbb{S}^{n-2}$. Then, we have*

$$\int_{\mathbb{S}^{n-2}} v^{\otimes(2k+1)} dv = 0, \quad \forall k \in \mathbb{N}, \tag{4.11}$$

$$\int_{\mathbb{S}^{n-2}} v \otimes v dv = \frac{1}{n-1} P_{\Omega^\perp}, \tag{4.12}$$

$$\int_{\mathbb{S}^{n-2}} v \otimes v \otimes v \otimes v dv = \frac{1}{(n-1)(n+1)} \Gamma, \tag{4.13}$$

where Γ is given in (2.28).

The proof of Lemma 4.3 can be found in Lemma 4.1 of [19]. Thus, we skip it here.

Now, with these preliminary results, we first present the limit of f^ε as $\varepsilon \rightarrow 0$.

4.2 Limit for f^ε

Lemma 4.4 (Limit of f^ε and $\rho_{f^\varepsilon} Q_{f^\varepsilon}$). *Let f^ε be the solution of Equation (2.4). Under Assumption 2.14, we have that*

$$f^\varepsilon(t, x, u) \rightarrow \rho(t, x) G_{\eta(\rho)A_\Omega}(t, x) \quad \text{as } \varepsilon \rightarrow 0,$$

for any (t, x) such that $\rho(t, x) > \rho_*$, for ρ_* as given in Proposition 2.9. Moreover, in this same regime of (t, x) , it also holds that

$$\rho_{f^\varepsilon} Q_{f^\varepsilon} \rightarrow \frac{\eta(\rho)}{\alpha} A_\Omega, \quad \text{as } \varepsilon \rightarrow 0, \tag{4.14}$$

where α is given in (2.8), $\eta = \eta(\rho)$ is given in (2.13), and A_Ω is given in (2.9).

Proof. By Assumption 2.14, f^ε converges to some function f^0 as $\varepsilon \rightarrow 0$. At the same time, from Equation (2.6) we have that $C(f^\varepsilon) = \mathcal{O}(\varepsilon^a)$ with $a \in (0, 2]$ and thus, taking the limit, $C(f^0) = 0$ as $\varepsilon \rightarrow 0$. Therefore, the limit f^0 must belong to the kernel of the operator C , which was characterized in Lemma 2.10. Therefore, we conclude that $f^0 = \rho(t, x) G_{\eta(\rho)A_\Omega}(t, x)$ for any (t, x) such that $\rho(t, x) > \rho_*$ and for some $\Omega \in \mathbb{S}^{n-1}$. Finally, the limit (4.14) is a direct consequence of (2.15) in Lemma 2.10. □

4.3 Derivation of Equation (2.17a)

Integrating the kinetic equation (2.6) with respect to u , and using Lemma 4.4 in the limit $\varepsilon \rightarrow 0$, we obtain

$$\partial_t \rho + \frac{\mu \chi^2}{\alpha} \nabla_x \cdot \left(\rho \int_{\mathbb{S}^{n-1}} (\nabla_x (u \cdot (\eta(\rho) A_\Omega) u) G_{\eta(\rho) A_\Omega}) \, du \right) + \mu \left(\frac{\chi^2}{n} - 1 \right) \nabla_x \cdot (\rho \nabla_x \rho) - D_x \Delta_x \rho = 0. \quad (4.15)$$

Notice that, above, we used the facts that the term in B_f vanishes and $\int_{\mathbb{S}^{n-1}} C(f^\varepsilon) \, du = 0$ for all $\varepsilon > 0$, both thanks to the divergence theorem.

Next, we compute the integral in the second term of (4.15),

$$\begin{aligned} & \int_{\mathbb{S}^{n-1}} \nabla_x (\eta(\rho) u \cdot A_\Omega u) G_{\eta(\rho) A_\Omega} \, du \\ &= \int_{\mathbb{S}^{n-1}} \nabla_x \left(\eta(\rho) \left[(u \cdot \Omega)^2 - \frac{1}{n} \right] \right) G_{\eta(\rho) A_\Omega} \, du \\ &= \int_{\mathbb{S}^{n-1}} \nabla_x \eta(\rho) \left((u \cdot \Omega)^2 - \frac{1}{n} \right) G_{\eta(\rho) A_\Omega} \, du + \int_{\mathbb{S}^{n-1}} 2\eta(\rho) (u \cdot \Omega) (u \cdot \nabla_x \Omega) G_{\eta(\rho) A_\Omega} \, du \\ &= \frac{n-1}{n} S_2(\eta) \nabla_x \eta(\rho), \end{aligned}$$

where in the last equality we used the fact that the second integral is zero. This can be computed similarly as for the integral in Equation (4.5) for $k = 1$ and $w = \partial \Omega$ with $\partial \Omega \perp \Omega$ (remembering that the matrix $\nabla_x \Omega$ is such that component-wise it corresponds to $(\nabla_x \Omega)_{ij} = \partial_{x_j} \Omega_i$).

Finally, substituting this last expression into (4.15) and using that $\nabla_x \eta(\rho) = \eta'(\rho) \nabla_x \rho$, we can combine the terms and obtain Equation (2.17a) for the mass density ρ .

4.4 Derivation of Equation (2.17b).

Classically, to obtain macroscopic equations from kinetic equations, one needs to find functions $\psi = \psi(u)$ that are collision invariant for the operator C , i.e., functions ψ such that, for all f , the following holds:

$$\int_{\mathbb{S}^{n-1}} C(f) \psi(u) \, du = 0.$$

The collision invariants correspond to conserved quantities. Typically, the number of macroscopic equations we obtain is the same as the number of collision invariants. For example, in our case, if ψ is a constant, then ψ is a collision invariant, which is related to the conservation of mass. Therefore, to obtain an equation of the mean-nematic direction Ω , we would like to find its associated collision invariant(s). However, Ω does not have any associated conserved quantity, i.e., one can check that the only collision invariants for our operator C , given in (2.7), are the constants [14].

To overcome this difficulty, the concept of Generalized Collision Invariant (GCI) was introduced in [21] for a model of collective dynamics where the momentum is not preserved. This idea, then, has been applied to other models of collective dynamics, see, e.g., [16, 19]. Moreover, the GCI for the operator C was already computed in [14]. Next, we state the main result regarding the GCI that we will be using in the sequel. The original source [14] contains a full proof of it.

Proposition 4.5 (Generalized Collision Invariant defined in [14] and Proposition 9 in [14]). *Let $f: \mathbb{S}^{n-1} \rightarrow \mathbb{R}$ be twice continuously differentiable such that $Q_f \neq 0$ and Q_f is the Q -tensor. Since Q_f is a symmetric matrix, all its eigenvalues are real. Suppose that the largest eigenvalue of Q_f is*

unique and denote Ω_f as the associated normalized eigenvector (which is unique up to sign). Then it holds that

$$\int_{\mathbb{S}^{n-1}} C(f) \psi_{\eta_f, \Omega_f} du = 0, \quad \text{for} \quad \psi_{\eta_f, \Omega_f} := h_{\eta_f}(u \cdot \Omega_f) P_{\Omega_f^\perp} u,$$

where h_η is the unique solution of

$$-(1-r^2)^{\frac{n-1}{2}} e^{\eta r^2} (2\eta r^2 + n-1) h_\eta + \frac{d}{dr} \left[(1-r^2)^{\frac{n+1}{2}} e^{\eta r^2} \frac{dh}{dr} \right] = r(1-r^2)^{\frac{n-1}{2}} e^{\eta r^2},$$

in the functional space

$$\mathcal{H} = \left\{ h : (-1, 1) \rightarrow \mathbb{R} \mid \int_{-1}^1 (1-r^2)^{\frac{n-1}{2}} |h(r)|^2 dr < \infty, \int_{-1}^1 (1-r^2)^{\frac{n+1}{2}} |h'(r)|^2 dr < \infty \right\}.$$

Moreover, h_η is an odd function with $h_\eta(r) \leq 0$ for $r \geq 0$.

A characterization of the GCI is given by the following definition and can be found in [14]:

Definition 4.6. Let $(\eta, \Lambda) \in (0, \infty) \times \mathcal{U}_n^0$. Then, we define the function $\psi_{\eta\Lambda} : \mathbb{S}^{n-1} \rightarrow \mathbb{R}^n$ as the unique solution (in $H^1(\mathbb{S}^{n-1}) = \{k \in H(\mathbb{S}^{n-1}) \mid \int_{\mathbb{S}^{n-1}} k(u) du = 0\}$) of the following equation:

$$\nabla_u \cdot (G_{\eta\Lambda}(u) \nabla_u \psi_{\eta\Lambda}) = (u \cdot \Omega_\Lambda) P_{\Omega_\Lambda^\perp} u G_{\eta\Lambda}(u) \quad \forall u \in \mathbb{S}^{n-1},$$

where \mathcal{U}_n^0 is the set of symmetric trace-free $n \times n$ -matrices whose principal eigenvalue is equal to $\frac{n-1}{n}$ and is simple.

Thanks to the GCI for the collision operator C we can now derive an equation for the mean-nematic direction Ω . Therefore, we multiply the kinetic equation given in (2.4) by $\psi_{\eta\Omega_f}$ and integrate with respect to u . Then, the term in C vanishes by the previous proposition. Therefore, we state the following result:

Proposition 4.7. Under the assumptions of Theorem 2.16, it holds that

$$\int_{\mathbb{S}^{n-1}} \mathcal{F}_u(\rho G_{\eta(\rho)A_\Omega}) \psi(u) du = 0, \quad \text{for} \quad \psi(u) = h_{\eta(\rho)}(u \cdot \Omega) P_{\Omega^\perp} u, \quad (4.16)$$

where $\eta = \eta(\rho)$ is given by (2.13), $h_\eta = h_{\eta(\rho)}(u \cdot \Omega)$ is defined in Proposition 4.5 and $\mathcal{F}_u(f)$ is defined as

$$\begin{aligned} \mathcal{F}_u(f) = & \partial_t f + \mu \chi^2 \nabla_x \cdot (\nabla_x (u^T \rho_f Q_f u) f) \\ & + \mu \left(\frac{\chi^2}{n} - 1 \right) \nabla_x \cdot ((\nabla_x \rho_f) f) - \lambda \mathbf{1}_{a=2} \nabla_u \cdot ((\nabla_u B_f) f) - D_x \Delta_x f. \end{aligned}$$

Proof. The proof is a direct consequence of Assumption 2.14, Lemma 4.4 and Proposition 4.5. \square

4.4.1 Limit of the terms not involving B_f

Now, we have all the ingredients to derive the macroscopic equation for Ω in a straightforward way. We apply Lemma 4.4 in the limit as $\varepsilon \rightarrow 0$ and rewrite Equation (4.16) as

$$I_1 + \mu \sigma I_2 + \mu \left(\frac{\chi^2}{n} - 1 \right) I_3 - \lambda \mathbf{1}_{a=2} I_4 - D_x I_5 = 0, \quad (4.17)$$

where

$$\begin{aligned}
I_1 &= \int_{\mathbb{S}^{n-1}} \partial_t (\rho G_{\eta(\rho)A\Omega}) \psi(u) \, du, \\
I_2 &= \int_{\mathbb{S}^{n-1}} \nabla_x \cdot (\nabla_x (u \cdot \eta(\rho)A\Omega u) \rho G_{\eta(\rho)A\Omega}) \psi(u) \, du, \\
I_3 &= \int_{\mathbb{S}^{n-1}} \nabla_x \cdot ((\nabla_x \rho) \rho G_{\eta(\rho)A\Omega}) \psi(u) \, du, \\
I_4 &= \int_{\mathbb{S}^{n-1}} \nabla_u \cdot \left(\nabla_u \left(B_{\rho G_{\eta(\rho)A\Omega}} \right) \rho G_{\eta(\rho)A\Omega} \right) \psi(u) \, du, \\
I_5 &= \int_{\mathbb{S}^{n-1}} \Delta_x (\rho G_{\eta(\rho)A\Omega}) \psi(u) \, du.
\end{aligned}$$

Notice that while writing I_2 we used (2.15). In this section, we will focus only on the terms I_1, I_2, I_3 and I_5 since the term I_4 appears exclusively if we choose $a = 2$. We will compute I_4 in the next section.

Lemma 4.8. *The following equalities hold:*

$$\begin{aligned}
I_1 &= \frac{2\eta(\rho)c_{1,2}}{n-1} \rho \partial_t \Omega, \\
I_2 &= \frac{2\eta(\rho)c_{1,2}}{n-1} \left(2 \frac{\eta'(\rho)}{\eta(\rho)} \rho + 1 + \rho \eta'(\rho) \left(2 \frac{c_{3,2}}{c_{1,2}} - \frac{1}{n} - d_{2,0} \right) \right) (\nabla_x \rho \cdot \nabla_x) \Omega + \frac{2\eta(\rho)c_{1,2}}{n-1} \rho P_{\Omega^\perp} \Delta_x \Omega, \\
I_3 &= \frac{2\eta(\rho)c_{1,2}}{n-1} \rho (\nabla_x \rho \cdot \nabla_x) \Omega, \\
I_5 &= \frac{2\eta(\rho)c_{1,2}}{n-1} \rho P_{\Omega^\perp} \Delta_x \Omega + \frac{2\eta(\rho)c_{1,2}}{n-1} 2 \left(\rho \eta' \left(\frac{1}{\eta(\rho)} + \frac{c_{3,2}}{c_{1,2}} - d_{2,0} \right) + 1 \right) (\nabla_x \rho \cdot \nabla_x) \Omega.
\end{aligned}$$

Proof. We start with computing I_1 ,

$$I_1 = \int_{\mathbb{S}^{n-1}} \partial_t (\rho G_{\eta(\rho)A\Omega}) \psi(u) \, du = \partial_t \rho \int_{\mathbb{S}^{n-1}} G_{\eta(\rho)A\Omega} \psi(u) \, du + \rho \int_{\mathbb{S}^{n-1}} \partial_t G_{\eta(\rho)A\Omega} \psi(u) \, du.$$

The first integral above on the last part of the equality is of the form (4.4) for $k = 0$, so it is zero. The second integral is of the form (4.6) for $k = 0$ and so I_1 becomes

$$I_1 = \frac{2\eta(\rho)c_{1,2}(\rho)}{n-1} \rho \partial_t \Omega.$$

Next, we compute I_2 ,

$$\begin{aligned}
I_2 &= \int_{\mathbb{S}^{n-1}} \nabla_x \cdot (\nabla_x (u \cdot \eta(\rho)A\Omega u) \rho G_{\eta(\rho)A\Omega}) \psi(u) \, du \\
&= \int_{\mathbb{S}^{n-1}} \Delta_x (u \cdot \eta(\rho)A\Omega u) \rho G_{\eta(\rho)A\Omega} \psi(u) \, du + \int_{\mathbb{S}^{n-1}} \nabla_x (u \cdot \eta(\rho)A\Omega u) \cdot \nabla_x \rho G_{\eta(\rho)A\Omega} \psi(u) \, du \\
&\quad + \rho \int_{\mathbb{S}^{n-1}} \nabla_x (u \cdot \eta(\rho)A\Omega u) \cdot \nabla_x G_{\eta(\rho)A\Omega} \psi(u) \, du =: I_2^1 + I_2^2 + I_2^3.
\end{aligned}$$

Proceeding further, we compute each I_2^i , $i \in \{1, 2, 3\}$ separately. Using (2.9), we have

$$u \cdot \eta(\rho)A\Omega u = \eta(\rho) \left((u \cdot \Omega)^2 - \frac{1}{n} \right).$$

The Laplacian of this expression reads

$$\begin{aligned}\Delta_x(u \cdot \eta(\rho)A_\Omega u) &= \Delta_x \eta(\rho) \left((u \cdot \Omega)^2 - \frac{1}{n} \right) + 4\nabla_x \eta(\rho) \cdot (u \cdot \Omega)(u \cdot \nabla_x \Omega) \\ &\quad + 2\eta(\rho)(u \cdot \nabla_x \Omega)^2 + 2\eta(\rho)(u \cdot \Omega)(u \cdot \Delta_x \Omega).\end{aligned}$$

Subsequently, using this, we obtain

$$\begin{aligned}I_2^1 &= \int_{\mathbb{S}^{n-1}} \Delta_x(u \cdot \eta(\rho)A_\Omega u) \rho G_{\eta(\rho)A_\Omega} \psi(u) du \\ &= \rho \Delta_x \eta(\rho) \int_{\mathbb{S}^{n-1}} \left((u \cdot \Omega)^2 - \frac{1}{n} \right) G_{\eta(\rho)A_\Omega} \psi(u) du \\ &\quad + 4\eta'(\rho) \rho \sum_{i=1}^n \partial_{x_i} \rho \left(\int_{\mathbb{S}^{n-1}} (u \cdot \Omega)(u \cdot \partial_{x_i} \Omega) G_{\eta(\rho)A_\Omega} \psi(u) du \right) \\ &\quad + 2\eta(\rho) \rho \int_{\mathbb{S}^{n-1}} (u \cdot \nabla_x \Omega)^2 G_{\eta(\rho)A_\Omega} \psi(u) du + 2\eta(\rho) \rho \int_{\mathbb{S}^{n-1}} (u \cdot \Omega)(u \cdot \Delta_x \Omega) G_{\eta(\rho)A_\Omega} \psi(u) du.\end{aligned}$$

We further simplify each integral above. The first and the third integrals are equal to zero as they are of the forms (4.4) for $k = 2$ and $k = 0$ and (4.8) for $k = 2$, respectively. The second and the fourth integrals are of the form (4.5) with $k = 1$ (and recall (4.10)). Combining these we obtain

$$I_2^1 = 4\eta'(\rho) \rho \frac{c_{1,2}}{n-1} (\nabla_x \rho \cdot \nabla_x) \Omega + 2\eta(\rho) \rho \frac{c_{1,2}}{n-1} P_{\Omega^\perp} \Delta_x \Omega.$$

Next, for I_2^2 we have

$$\begin{aligned}I_2^2 &= \nabla_x \rho \cdot \int_{\mathbb{S}^{n-1}} \nabla_x(u \cdot \eta(\rho)A_\Omega u) G_{\eta(\rho)A_\Omega} \psi(u) du \\ &= |\nabla_x \rho|^2 \eta'(\rho) \int_{\mathbb{S}^{n-1}} \left((u \cdot \Omega)^2 - \frac{1}{n} \right) G_{\eta(\rho)A_\Omega} \psi(u) du \\ &\quad + 2\eta(\rho) \sum_{i=1}^n \partial_{x_i} \rho \left(\int_{\mathbb{S}^{n-1}} (u \cdot \Omega)(u \cdot \partial_{x_i} \Omega) G_{\eta(\rho)A_\Omega} \psi(u) du \right).\end{aligned}$$

Noticing that the first integral above is of the form (4.4) with $k = 2$ and $k = 0$ and the second integral is of the form (4.5) with $k = 1$ and recalling (4.10), we conclude

$$I_2^2 = 2\eta(\rho) \frac{c_{1,2}}{n-1} (\nabla_x \rho \cdot \nabla_x) \Omega.$$

Similarly, we obtain (here we additionally use (4.3) for $\nabla_x G_{\eta(\rho)A_\Omega}$)

$$\begin{aligned}I_2^3 &= \rho \int_{\mathbb{S}^{n-1}} \nabla_x(u \cdot \eta(\rho)A_\Omega u) \cdot \nabla_x G_{\eta(\rho)A_\Omega} \psi(u) du \\ &= \rho \eta'(\rho) \sum_{i=1}^n \partial_{x_i} \rho \int_{\mathbb{S}^{n-1}} \left((u \cdot \Omega)^2 - \frac{1}{n} \right) \partial_{x_i} G_{\eta(\rho)A_\Omega} \psi(u) du \\ &\quad + 2\eta(\rho) \rho \int_{\mathbb{S}^{n-1}} (u \cdot \Omega) ((u \cdot \nabla_x \Omega) \cdot \nabla_x G_{\eta(\rho)A_\Omega}) \psi(u) du.\end{aligned}$$

The first integral above is of the form (4.6) for $k = 2$ and $k = 0$ (for the terms $(u \cdot \Omega)^2$ and $1/n$), respectively; and the second integral is of the form (4.7) for $k = 1$, therefore, we have that

$$I_2^3 = 2\rho \eta(\rho) \eta'(\rho) \left(\frac{2c_{3,2} - c_{1,2}/n - d_{2,0}c_{1,2}}{n-1} \right) (\nabla_x \rho \cdot \nabla_x) \Omega.$$

Combining these we compute I_3 analogously to obtain

$$I_3 = \int_{\mathbb{S}^{n-1}} \nabla_x \cdot ((\nabla_x \rho) \rho G_{\eta(\rho)A\Omega}) \psi(u) \, du = 2\rho\eta(\rho) \frac{c_{1,2}}{n-1} (\nabla_x \rho \cdot \nabla_x) \Omega.$$

Finally, for I_5 we have

$$\begin{aligned} I_5 &= \int_{\mathbb{S}^{n-1}} \Delta_x (\rho G_{\eta(\rho)A\Omega}) \psi(u) \, du \\ &= \Delta_x \rho \int_{\mathbb{S}^{n-1}} G_{\eta(\rho)A\Omega} \psi(u) \, du + 2 \sum_{j=1}^n \partial_{x_d} \rho \int_{\mathbb{S}^{n-1}} \partial_{x_d} G_{\eta(\rho)A\Omega} \psi(u) \, du + \rho \int_{\mathbb{S}^{n-1}} \Delta_x G_{\eta(\rho)A\Omega} \psi(u) \, du. \end{aligned}$$

The first integral above is of the form (4.4) for $k = 0$, so it is zero; the second integral is of the form (4.6) for $k = 0$; for the third integral we use (4.9) and that $\partial \eta = \eta'(\rho) \partial(\rho)$. Hence, we conclude

$$I_5 = \frac{2c_{1,2}}{n-1} \eta(\rho) \rho P_{\Omega^\perp} \Delta_x \Omega + \frac{4}{n-1} (\rho \eta' [c_{1,2} + \eta(c_{3,2} - d_{2,0} c_{1,2})] + \eta(\rho) c_{1,2}) (\nabla_x \rho \cdot \nabla_x) \Omega.$$

This completes the proof. \square

4.4.2 Limit of the term with B_f

In this section, we compute the remaining integral I_4 in Equation (4.17), which includes the term B_f . First, we prove the following lemma:

Lemma 4.9. *Let B_f be given by (2.3) with $f = \rho G_{\eta(\rho)A\Omega}$. Then the following holds*

$$\int_{\mathbb{S}^{n-1}} \nabla_u \cdot (\nabla_u B_{\rho G_{\eta(\rho)A\Omega}} \rho G_{\eta A\Omega}) h_\eta(u \cdot \Omega) P_{\Omega^\perp} u \, du = \rho \int_{\mathbb{S}^{n-1}} B_{\rho G_{\eta(\rho)A\Omega}}(u) (u \cdot \Omega) P_{\Omega^\perp} u G_{\eta A\Omega} \, du.$$

Proof. Applying integration by parts twice, we rewrite the integral as

$$\begin{aligned} &\int_{\mathbb{S}^{n-1}} \nabla_u \cdot (\nabla_u B_{\rho G_{\eta(\rho)A\Omega}} \rho G_{\eta A\Omega}) h_\eta(u \cdot \Omega) P_{\Omega^\perp} u \, du \\ &= - \int_{\mathbb{S}^{n-1}} (\nabla_u B_{\rho G_{\eta(\rho)A\Omega}} \rho G_{\eta A\Omega}) \cdot \nabla_u [h_\eta(u \cdot \Omega) P_{\Omega^\perp} u] \, du \\ &= \rho \int_{\mathbb{S}^{n-1}} B_{\rho G_{\eta(\rho)A\Omega}} \nabla_u \cdot (G_{\eta A\Omega} \nabla_u [h_\eta(u \cdot \Omega) P_{\Omega^\perp} u]) \, du. \end{aligned}$$

We conclude the result since the GCI $\psi = h_\eta(u \cdot \Omega) P_{\Omega^\perp} u$ satisfies

$$\nabla_u \cdot (G_{\eta A\Omega} \nabla_u \psi) = (u \cdot \Omega) P_{\Omega^\perp} u G_{\eta A\Omega}$$

by Definition 4.6. \square

Now, we go back to Equation (4.17) to rewrite I_4 using Lemma 4.9,

$$I_4 = \rho \int_{\mathbb{S}^{n-1}} B_{\rho G_{\eta(\rho)A\Omega}}(u) (u \cdot \Omega) P_{\Omega^\perp} u G_{\eta A\Omega} \, du. \quad (4.18)$$

First, we recast $B_{\rho G_{\eta(\rho)A\Omega}} = [B] + [B]_{\text{even}}$, as stated in Equation (2.3), by expanding

$$\Sigma(u, u_2) = (\ell^2 - d^2)(u \otimes u) + (\ell^2 - d^2)(u_2 \otimes u_2) + 2d^2 \text{Id}$$

and the factor $(1 - \chi^2(u \cdot u_2)^2)$. Hence, we obtain

$$\begin{aligned} [B] &:= \frac{(\ell^2 - d^2)}{4} ((u \otimes u) : D_x^2) \rho - \frac{\chi^2}{4} (\ell^2 - d^2) \int_{\mathbb{S}^{n-1}} (u \cdot u_2)^2 ((u \otimes u) : D_x^2) (\rho G_{\eta(\rho)A_\Omega}(u_2)) \, du_2 \\ &\quad - \frac{\chi^2}{4} (\ell^2 - d^2) \int_{\mathbb{S}^{n-1}} (u \cdot u_2)^2 ((u_2 \otimes u_2) : D_x^2) (\rho G_{\eta(\rho)A_\Omega}(u_2)) \, du_2 \\ &\quad - \frac{\chi^2}{2} d^2 \int_{\mathbb{S}^{n-1}} (u \cdot u_2)^2 \Delta_x (\rho G_{\eta(\rho)A_\Omega}(u_2)) \, du_2. \end{aligned}$$

and

$$[B]_{\text{even}} := \frac{(\ell^2 - d^2)}{4} \int_{\mathbb{S}^{n-1}} ((u_2 \otimes u_2) : D_x^2) (\rho G_{\eta(\rho)A_\Omega}(u_2)) \, du_2 + \frac{d^2}{2} \Delta_x \rho.$$

Now, using the change of variables (4.1) in (4.18), we have that

$$I_4 = \rho \int_{\mathbb{S}^{n-2}} v \int_0^\pi B_{\rho G_{\eta(\rho)A_\Omega}}(u(\theta)) \cos \theta \sin \theta \, g_\eta(\theta) \sin^{d-2} \theta \, d\theta \, dv.$$

Notice that the terms in $[B]_{\text{even}}$ are independent of u , so they have zero contribution to I_4 (since they give an integrand odd in v). Now, we rewrite I_4 using $[B]$ and the tensor product:

$$\begin{aligned} I_4 &= \rho \frac{(\ell^2 - d^2)}{4} [(H_2^r : D_x^2)]_{[2,3,1,2]} \rho - \rho \frac{\chi^2}{4} (\ell^2 - d^2) [H_4^r : (D_x^2 \otimes (\rho H_2))]_{[2,3,4,5:1,2,3,4]} \\ &\quad - \rho \frac{\chi^2}{4} (\ell^2 - d^2) [H_2^r \otimes D_x^2 : (\rho H_4)]_{[2,3,4,5:1,2,3,4]} - \rho \frac{\chi^2}{2} d^2 [H_2^r : \Delta_x (\rho H_2)]_{[2,3:1,2]}, \end{aligned}$$

where in the second term above, the s -th component of the contraction is defined as

$$([H_4^r : (D_x \otimes (\rho H_2))]_{[2,3,4,5:1,2,3,4]})_s = \sum_{i,j,k,p} (H_4^r)_{sijkp} \partial_{x_i} \partial_{x_j} (\rho (H_2)_{kp})$$

and analogously for the other contractions; and where

$$\begin{aligned} H_2 &= H_2(\eta, \Omega, \Omega^\perp) = \int_{\mathbb{S}^{n-1}} (u \otimes u) G_{\eta A_\Omega} \, du, \\ H_2^r &= H_2^r(\eta, \Omega, \Omega^\perp) = \int_{\mathbb{S}^{n-1}} P_{\Omega^\perp} u \otimes (u \otimes u) (u \cdot \Omega) G_{\eta A_\Omega} \, du, \\ H_4 &= H_4(\eta, \Omega, \Omega^\perp) = \int_{\mathbb{S}^{n-1}} (u \otimes u \otimes u \otimes u) G_{\eta A_\Omega} \, du, \\ H_4^r &= H_4^r(\eta, \Omega, \Omega^\perp) = \int_{\mathbb{S}^{n-1}} P_{\Omega^\perp} u \otimes (u \otimes u \otimes u \otimes u) (u \cdot \Omega) G_{\eta A_\Omega} \, du. \end{aligned}$$

We can now rewrite these terms in such a way that they only depend on Ω , Ω^\perp and η .

Lemma 4.10 (Dimension $n = 2$). *In case of only $n = 2$, we have that H_2, H_2^r, H_4, H_4^r correspond to expressions (2.22), (2.23), (2.24) and (2.25), respectively.*

The proof of this lemma is based on the change of variables (4.1) for $n = 2$, i.e., $u = \cos \theta \Omega + \sin \theta \Omega^\perp$, and the same type of argument as in the proof of Lemma 4.2. Thus, we skip it here.

We conclude this section by computing the values of H_2, H_2^r, H_4, H_4^r in dimension $n \geq 3$:

Proof of Proposition 2.17. For this proof, we consider the decomposition of $u \in \mathbb{S}^{n-1}$ into

$$u = u_{\parallel} + u_{\perp}, \quad u_{\parallel} := P_{\Omega}u = (u \cdot \Omega)\Omega, \quad u_{\perp} := P_{\Omega^{\perp}}u,$$

and the change of variables given in (4.1) where we have that

$$(u \cdot \Omega) = \cos \theta, \quad P_{\Omega^{\perp}}u = \sin \theta v.$$

Then, the proof of this lemma closely the proof of Lemma 4.1 in [19]. There, the authors prove that,

$$\mathcal{A}_{ij} := \int_{\mathbb{S}^{n-1}} \phi(u \cdot \Omega)(u_{\perp})_i(u_{\perp})_j \, du = \frac{1}{n-1} \left(\int_{\mathbb{S}^{n-1}} \phi(u \cdot \Omega)(1 - (u \cdot \Omega)^2) \, du \right) (P_{\Omega^{\perp}})_{ij} \quad (4.19)$$

where $\phi = \phi(u \cdot \Omega)$ is a given function. The authors also consider

$$S_{ijkl} := \int_{\mathbb{S}^{n-1}} \phi(u \cdot \Omega)(u_{\perp})_i(u_{\perp})_j(u_{\perp})_k(u_{\perp})_l \, du.$$

and we additionally define

$$C_S := \frac{1}{(n-1)(n+1)} \int_{\mathbb{S}^{n-1}} \phi(u \cdot \Omega)(1 - (u \cdot \Omega)^2)^2 \, du.$$

Notice that the only non-zero terms correspond to

$$S_{iii} = 3C_S \Gamma_{iii}, \quad S_{ijj} = C_S \Gamma_{ijj}, \quad S_{jij} = C_S \Gamma_{ijj}, \quad S_{jji} = C_S \Gamma_{ijj},$$

where Γ is given in (2.28) and $i, j \in \{1, \dots, n\}$ such that $i \neq j$. With this we are ready to carry out the proof.

The equality for H_2 in (2.26) is obtained by proceeding similarly as in the proof of Lemma 4.2 and using (4.12).

Next, we look at H_2^r to prove (2.27). We have that

$$\begin{aligned} H_2^r &= \int_{\mathbb{S}^{n-1}} u_{\perp} \otimes (u_{\perp} \otimes u_{\parallel})(u \cdot \Omega) G_{\eta(\rho)A_{\Omega}} \, du + \int_{\mathbb{S}^{n-1}} u_{\perp} \otimes (u_{\parallel} \otimes u_{\perp})(u \cdot \Omega) G_{\eta(\rho)A_{\Omega}} \, du \\ &= \frac{d_{2,2}}{n-1} P_{\Omega^{\perp}} \Omega + R_2^r. \end{aligned}$$

with $d_{2,2}$ given in Equation (2.20).

In the first equality above, the integrands that are odd in u_{\perp} vanish (analogously to what happens when performing the change of variables (4.1): the terms that are odd in v vanish). In the second equality, for the first integral we used (4.12) and for the second integral we define

$$\begin{aligned} (R_2^r)_{ijk} &= \int_{\mathbb{S}^{n-1}} (u_{\perp})_i(u_{\parallel})_j(u_{\perp})_k(u \cdot \Omega) G_{\eta(\rho)A_{\Omega}} \, du = \Omega_j \int (u_{\perp})_i(u_{\perp})_k(u \cdot \Omega)^2 G_{\eta(\rho)A_{\Omega}} \, du \\ &= \Omega_j \mathcal{A}_{ik} = \Omega_j \frac{d_{2,2}}{n-1} (P_{\Omega^{\perp}})_{ik}, \end{aligned}$$

where in the definition of \mathcal{A} we used $\phi(u \cdot \Omega) = (u \cdot \Omega)^2 G_{\eta(\rho)A_{\Omega}}$.

Now consider

$$([P_{\Omega^{\perp}} \otimes \Omega \otimes P_{\Omega^{\perp}}]_{:24})_{ijk} = \sum_{p=1}^n (P_{\Omega^{\perp}})_{ip} \Omega_j (P_{\Omega^{\perp}})_{pk} = \Omega_j (P_{\Omega^{\perp}})_{ik},$$

where the second equality is a straightforward computation. Therefore, we conclude that

$$R_2^r = \frac{d_{2,2}}{n-1} [P_{\Omega^\perp} \otimes \Omega \otimes P_{\Omega^\perp}]:_{24}.$$

We proceed by focusing on H_4 and expanding it:

$$\begin{aligned} H_4 &= \int_{\mathbb{S}^{n-1}} (u_\perp \otimes u_\perp \otimes u_\perp \otimes u_\perp) G_{\eta(\rho)A_\Omega} \, du + \int_{\mathbb{S}^{n-1}} (u_\perp \otimes u_\perp \otimes u_\parallel \otimes u_\parallel) G_{\eta(\rho)A_\Omega} \, du \\ &+ \int_{\mathbb{S}^{n-1}} (u_\parallel \otimes u_\parallel \otimes u_\perp \otimes u_\perp) G_{\eta(\rho)A_\Omega} \, du + \int_{\mathbb{S}^{n-1}} (u_\parallel \otimes u_\perp \otimes u_\perp \otimes u_\parallel) G_{\eta(\rho)A_\Omega} \, du \\ &+ \int_{\mathbb{S}^{n-1}} (u_\perp \otimes u_\parallel \otimes u_\perp \otimes u_\parallel) G_{\eta(\rho)A_\Omega} \, du + \int_{\mathbb{S}^{n-1}} (u_\perp \otimes u_\parallel \otimes u_\parallel \otimes u_\perp) G_{\eta(\rho)A_\Omega} \, du \\ &+ \int_{\mathbb{S}^{n-1}} (u_\parallel \otimes u_\perp \otimes u_\parallel \otimes u_\perp) G_{\eta(\rho)A_\Omega} \, du + \int_{\mathbb{S}^{n-1}} (u_\parallel \otimes u_\parallel \otimes u_\parallel \otimes u_\parallel) G_{\eta(\rho)A_\Omega} \, du \\ &=: D_1 + D_2 + D_3 + \dots + D_8, \end{aligned}$$

where all the terms odd in u_\perp vanished. Considering the change of variables (4.1), we deduce from (4.13) that

$$D_1 = d_{0,4} \frac{1}{(n-1)(n+1)} \Gamma.$$

From (4.12), (4.19) and proceeding as before, we have that

$$D_2 = \frac{d_{2,2}}{n-1} P_{\Omega^\perp} \otimes \Omega \otimes \Omega, \quad D_3 = \frac{d_{2,2}}{n-1} \Omega \otimes \Omega \otimes P_{\Omega^\perp}, \quad D_4 = \frac{d_{2,2}}{n-1} \Omega \otimes P_{\Omega^\perp} \otimes \Omega.$$

Furthermore, proceeding as in the computation for R_2^r we obtain

$$D_5 = \frac{d_{2,2}}{n-1} [P_{\Omega^\perp} \otimes \Omega \otimes P_{\Omega^\perp} \otimes \Omega]:_{24}, \quad D_6 = \frac{d_{2,2}}{n-1} [P_{\Omega^\perp} \otimes \Omega \otimes \Omega \otimes P_{\Omega^\perp}]:_{25},$$

$$D_7 = \frac{d_{2,2}}{n-1} [\Omega \otimes P_{\Omega^\perp} \otimes \Omega \otimes P_{\Omega^\perp}]:_{35}.$$

By applying the change of variables (4.1) to the last term we directly have that

$$D_8 = d_{4,0} \Omega \otimes \Omega \otimes \Omega \otimes \Omega$$

Finally, we split H_4^r into

$$H_4^r = D_9 + D_{10},$$

with

$$\begin{aligned} D_9 &= \int_{\mathbb{S}^{n-1}} (u_\perp \otimes (u_\perp \otimes u_\perp \otimes u_\perp \otimes u_\parallel)(u \cdot \Omega) + u_\perp \otimes (u_\perp \otimes u_\perp \otimes u_\parallel \otimes u_\perp)(u \cdot \Omega)) G_{\eta(\rho)A_\Omega} \, du \\ &+ \int_{\mathbb{S}^{n-1}} (u_\perp \otimes (u_\perp \otimes u_\parallel \otimes u_\perp \otimes u_\perp)(u \cdot \Omega) + u_\perp \otimes (u_\parallel \otimes u_\perp \otimes u_\perp \otimes u_\perp)(u \cdot \Omega)) G_{\eta(\rho)A_\Omega} \, du, \end{aligned}$$

and

$$\begin{aligned} D_{10} &= \int_{\mathbb{S}^{n-1}} (u_\perp \otimes (u_\perp \otimes u_\parallel \otimes u_\parallel \otimes u_\parallel)(u \cdot \Omega) + u_\perp \otimes (u_\parallel \otimes u_\perp \otimes u_\parallel \otimes u_\parallel)(u \cdot \Omega)) G_{\eta(\rho)A_\Omega} \, du \\ &+ \int_{\mathbb{S}^{n-1}} (u_\perp \otimes (u_\parallel \otimes u_\parallel \otimes u_\perp \otimes u_\parallel)(u \cdot \Omega) + u_\perp \otimes (u_\parallel \otimes u_\parallel \otimes u_\parallel \otimes u_\perp)(u \cdot \Omega)) G_{\eta(\rho)A_\Omega} \, du, \end{aligned}$$

where the terms odd in u_\perp vanished. Proceeding as in the computation of R_2^r we have that

$$D_{10} = \frac{d_{4,2}}{n-1} \left(P_{\Omega^\perp} \otimes \Omega \otimes \Omega \otimes \Omega + [P_{\Omega^\perp} \otimes \Omega \otimes P_{\Omega^\perp} \otimes \Omega \otimes \Omega]_{:24} \right. \\ \left. + [P_{\Omega^\perp} \otimes \Omega \otimes \Omega \otimes P_{\Omega^\perp} \otimes \Omega]_{:25} + [P_{\Omega^\perp} \otimes \Omega \otimes \Omega \otimes \Omega \otimes P_{\Omega^\perp}]_{:26} \right).$$

To compute D_9 , we consider the second component in the first integral as an example. This integral is a 5-tensor. We apply $u_\parallel = (u \cdot \Omega)\Omega$ and look at the components i, j, k, l, m

$$\left(\int_{\mathbb{S}^{n-1}} u_\perp \otimes (u_\perp \otimes u_\perp \otimes \Omega \otimes u_\perp) (u \cdot \Omega)^2 G_{\eta(\rho)A\Omega} du \right)_{ijklm} \\ = \int_{\mathbb{S}^{n-1}} (u_\perp)_i (u_\perp)_j (u_\perp)_k \Omega_l (u_\perp)_m (u \cdot \Omega)^2 G_{\eta(\rho)A\Omega} du = \Omega_l S_{ijklm},$$

where in the definition of S_{ijklm} we have $\phi(u \cdot \Omega) = (u \cdot \Omega)^2 G_{\eta(\rho)A\Omega}$, which in this case means that $C_S = d_{2,4}$. Putting all the terms of D_9 together and by considering all the combinations of indices we have that

$$D_9 = \frac{d_{2,4}}{(n-1)(n+1)} T,$$

with T given in (2.29). This completes the proof. \square

5 Conclusions

In this article, we have explored the effects of an anisotropic repulsive potential on inert particles. We derived both kinetic (2.4) and macroscopic equations (2.17a)-(2.17b) and discussed potential interpretations of the latter. The equation for the particle density ρ is independent of the particles' mean-nematic direction Ω . However, the anisotropy of the particles slows down the non-linear diffusion of the particle density ρ . In contrast, the equation for Ω is more complex and challenging to interpret. It consists of transport and diffusion terms, resulting from the effect of the repulsive potential on the particles' position. Additionally, the repulsive potential acting on the particles' direction creates a complex, diffusive-type operator with different signs for oblate and prolate particles.

Many models for collective dynamics impose an alignment force directly on particle directions. Our main goal in this article was to observe the nematic alignment and the spatial effects of the anisotropic Gaussian-type repulsive potential on the particle dynamics without imposing the alignment directly.

However, when we derived this effect directly from an anisotropic repulsive potential, we observed intriguing phenomena. For instance, we can understand how particle anisotropy influences the evolution of particle density, how particle positions affect their directions, and what the impact of the specific interaction potential considered on the directions is (through the term B_f).

The well-posedness of these equations will be the object of future studies, along with the consideration of other types of anisotropic repulsive potentials, such as generalizations of the Lennard-Jones potential. Another interesting aspect for future research is the study of compactly supported potentials, which may better represent contact interactions.

Acknowledgements

The authors would like to thank Pierre Degond for wonderful and fruitful discussions.

The work of SMA and CW was funded in part by the Austrian Science Fund (FWF) project [10.55776/F65](#) and in part by the Vienna Science and Technology Fund (WWTF) [[10.47379/VRG17014](#)].

CW was funded partly by the Austrian Science Fund (FWF) **W1261-B28**. SP is supported by the KAKENHI Grant-in-Aid for Early-Career Scientists (Grant number 24K16962). HY is supported by the Dutch Research Council (NWO) under the NWO-Talent Programme Veni ENW project MetaMathBio with the project number VI.Veni.222.288. This research was completed while HY was visiting the Okinawa Institute of Science and Technology (OIST) through the Theoretical Sciences Visiting Program (TSVP). SP gratefully acknowledges the hospitality of the TSVP during his stay at OIST.

A Appendices

A.1 Proof of Lemma 2.1

Proof. Considering the scaling $\ell = \varepsilon \ell'$ and $d = \varepsilon d'$ and a change of variable $z = \frac{x_2 - x_1}{\varepsilon}$, so $\varepsilon^n dz = dx_2$, we obtain

$$\begin{aligned} V_f(t, x_1, u_1) &= \int_{\mathbb{S}^{n-1}} \int_{\mathbb{R}^n} V_{b_{\text{WG}}} \left(u_1, u_2, \frac{x_2 - x_1}{\varepsilon} \right) f^\varepsilon(t, x_2, u_2) dx_2 du_2 \\ &= \varepsilon^n \int_{\mathbb{S}^{n-1}} \int_{\mathbb{R}^n} V_{b_{\text{WG}}}(u_1, u_2, z) f^\varepsilon(t, x_1 + \varepsilon z, u_2) dz du_2. \end{aligned}$$

Now, we perform a Taylor expansion of $f^\varepsilon(t, \cdot, u_2)$ at x_1 to obtain

$$f^\varepsilon(t, x_1 + \varepsilon z, u_2) = f^\varepsilon(t, x_1, u_2) + \varepsilon z \cdot \nabla_x f^\varepsilon(t, x_1, u_2) + \frac{1}{2} \varepsilon^2 z^T D_x^2 f^\varepsilon(t, x_1, u_2) \cdot z + \mathcal{O}(\varepsilon^3).$$

Since, we consider the weighted Gaussian potential $V_{b_{\text{WG}}}$, as defined in Equation (1.6), we use $\int_{\mathbb{R}^n} z V_{b_{\text{WG}}}(u_1, u_2, z) dz = 0$, and thus for the potential $V_f(t, x_1, u_1)$, we have that

$$\begin{aligned} V_f(t, x_1, u_1) &= \varepsilon^n \int_{\mathbb{S}^{n-1}} \left(\int_{\mathbb{R}^n} V_{b_{\text{WG}}}(u_1, u_2, z) dz \right) f^\varepsilon(t, x_1, u_2) du_2 \\ &\quad + \frac{\varepsilon^{n+2}}{2} \int_{\mathbb{S}^{n-1}} \int_{\mathbb{R}^n} V_{b_{\text{WG}}}(u_1, u_2, z) z^T D_x^2 f^\varepsilon(t, x_1, u_2) \cdot z dz du_2 + \mathcal{O}(\varepsilon^{n+3}). \end{aligned}$$

Notice that with the scaling factor (1.5) we have for the potential $V_{b_{\text{WG}}}$,

$$\begin{aligned} \int_{\mathbb{R}^n} V_{b_{\text{WG}}}(u_1, u_2, z) dz &= b_{\text{WG}}^2(u_1, u_2), \\ \int_{\mathbb{R}^n} (z \otimes z) V_{b_{\text{WG}}}(u_1, u_2, z) dz &= \frac{1}{2} b_{\text{WG}}^2(u_1, u_2) \Sigma. \end{aligned} \tag{A.1}$$

Using (A.1), we obtain

$$\begin{aligned} V_f(t, x_1, u_1) &= \varepsilon^n \int_{\mathbb{S}^{n-1}} (1 - \chi^2(u_1 \cdot u_2)^2) f(t, x_1, u_2) du_2 \\ &\quad + \frac{\varepsilon^{n+2}}{4} \int_{\mathbb{S}^{n-1}} (1 - \chi^2(u_1 \cdot u_2)^2) \Sigma(u_1, u_2) : D_x^2 f(t, x_1, u_2) du_2 + \mathcal{O}(\varepsilon^{n+3}). \end{aligned}$$

Then,

$$V_f^\varepsilon(t, x_1, u_1) = \frac{1}{\varepsilon^n} V_f(t, x_1, u_1) = W_f(t, x_1, u_1) + \varepsilon^2 B_f(t, x_1, u_1) + \mathcal{O}(\varepsilon^3).$$

where W_f and B_f are Equations (2.2) and (2.3) in the lemma. \square

A.2 Proof of Lemma 4.2

Proof. We will consider the change of variables given in (4.1) throughout the following proof and thus we can recast

$$\begin{aligned}\psi(u) &= h_\eta(\cos \theta) \sin \theta v, \\ G_{\eta(\rho)A_\Omega}(u) &= g_\eta(\theta),\end{aligned}$$

where $g_\eta(\theta)$ is given in (4.2).

To begin with, doing the change of variables (4.1), the integral (4.4) corresponds to

$$\int_{\mathbb{S}^{n-1}} (u \cdot \Omega)^k G_{\eta(\rho)A_\Omega} \psi(u) \, du = c_{k,1} \left(\int_{S^{n-2}} v \, dv \right).$$

The integral in v is zero since the integrand is odd. Moreover, the function $c_{k,p}$ is defined in (2.19).

Proceeding similarly, we consider (4.12) and transform (4.5) into

$$\int_{\mathbb{S}^{n-1}} (u \cdot w)(u \cdot \Omega)^k G_{\eta(\rho)A_\Omega} \psi(u) \, du = c_{k,2} \left(\int_{S^{n-2}} v \otimes v \, dv \right) w = \frac{c_{k,2}}{n-1} P_{\Omega^\perp} w.$$

Now, the integral (4.6) is computed analogously, since we know the value of $\partial G_{\eta(\rho)A_\Omega}$ from Lemma 4.1 and using that $P_{\Omega^\perp} \partial \Omega = \partial \Omega$.

Integral (4.7) is also computed analogously using relation (4.11).

Moreover, considering (4.11) we recast integral (4.8) as

$$\int_{\mathbb{S}^{n-1}} (u \cdot \Omega)^{2k} (u \cdot w)^2 G_{\eta(\rho)A_\Omega} \psi(u) \, du = 2(\Omega \cdot w) c_{2k+1,1} \left(\int_{S^{n-2}} v \otimes v \, dv \right) w,$$

and since $w \perp \Omega$ the integral vanishes.

Finally, the integral (4.9) is computed in the same way as above using the corresponding expression for $\partial^2 G_{\eta(\rho)A_\Omega}$ provided in Lemma 4.1. \square

A.3 Numerical approximation of $K(\eta)$ and additional figures

In the following, we outline the method we use to approximate the diffusion parameter $K(\eta)$ in Figures 3 and 10c. One can approximate $S_2(\eta)$ via applying numerical quadrature such as the adaptive Gauss–Kronrod quadrature to (2.12), we refer to this approximation as \tilde{S}_2 . Next, the function $\eta(\rho)$ can be interpolated by computing $\tilde{S}_2(\eta_j)$ at equidistant points $\eta_j = \frac{C(1-\chi^2)j}{m}$ for $1 \leq j \leq m$ where m is the number of interpolation points and $C > 0$ is a large enough constant. Using these points, one can define $\tilde{\eta}$ as the Akima interpolation of $\left(\frac{\eta_j}{\alpha \tilde{S}_2(\eta_j)}, \eta_j \right)$. The regularization effect of the Akima interpolation is useful to counter numerical instabilities for small values of η close to the unknown η^* . Finally, to approximate K , we evaluate

$$\tilde{K}(\rho) := 1 - \frac{\chi^2}{n} - \sigma \frac{n-1}{n} \tilde{S}_2(\tilde{\eta}(\rho)) \tilde{\eta}'(\rho)$$

where the derivative $\tilde{\eta}'$ is the derivative of the Akima interpolant.

We finish the appendices with some additional figures from our numerical experiments.

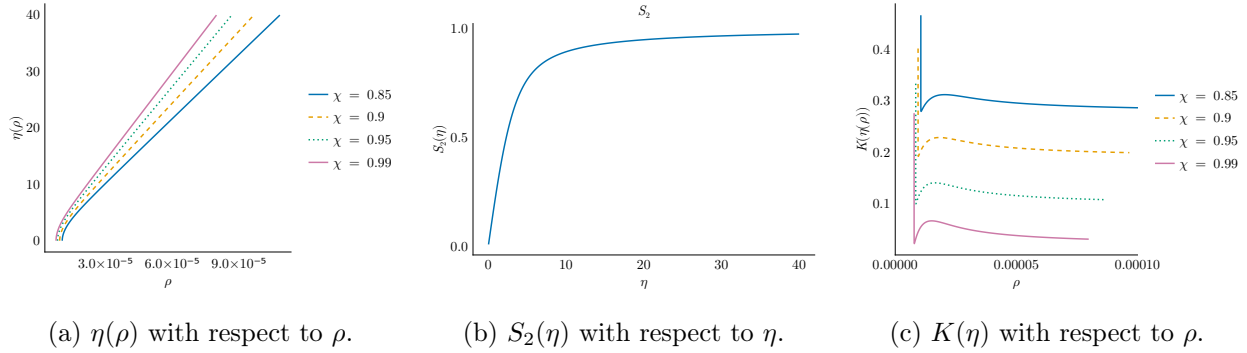


Figure 10: (a) Plots of $\eta(\rho)$ with respect to ρ , for different χ values corresponding to different colors. Notice that η is non-decreasing with respect to ρ . (b) A plot of $S_2(\eta)$ versus η . (c) Evolution of the diffusion coefficient K with respect to the particle density ρ . Different colors correspond to different χ values.

References

- [1] S. Alt, P. Ganguly, and G. Salbreux. Vertex models: from cell mechanics to tissue morphogenesis. *Philosophical Transactions of the Royal Society B*, 372(1720):20150520, 2017.
- [2] J. M. Ball. Mathematics and liquid crystals. *Molecular Crystals and Liquid Crystals*, 647(1):1–27, 2017.
- [3] A. Baskaran and M. C. Marchetti. Enhanced diffusion and ordering of self-propelled rods. *Physical Review Letters*, 101(26):268101, 2008.
- [4] A. Baskaran and M. C. Marchetti. Hydrodynamics of self-propelled hard rods. *Physical Review E*, 77(1):011920, 2008.
- [5] B. J. Berne and P. Pechukas. Gaussian model potentials for molecular interactions. *The Journal of Chemical Physics*, 56(8):4213–4216, 1972.
- [6] T. Bodineau, I. Gallagher, L. Saint-Raymond, and S. Simonella. *Dynamics of dilute gases: a statistical approach*, volume 2. European Mathematical Society, 2022. ICM Plenary Lectures.
- [7] M. Bodnar and J. J. L. Velázquez. Friction dominated dynamics of interacting particles locally close to a crystallographic lattice. *Mathematical Methods in the Applied Sciences*, 36(10):1206–1228, 2013.
- [8] R. Borsche, A. Klar, A. Meurer, and O. Tse. Mean field models for interacting ellipsoidal particles. *Computers & Mathematics with Applications*, 72(3):704–719, 2016.
- [9] M. Bruna, M. Burger, H. Ranetbauer, and M.-T. Wolfram. Cross-diffusion systems with excluded-volume effects and asymptotic gradient flow structures. *Journal of Nonlinear Science*, 27(2):687–719, 2017.
- [10] M. Bruna, S. J. Chapman, and M. Schmidtchen. Derivation of a macroscopic model for Brownian hard needles. *Proceedings of the Royal Society A: Mathematical, Physical and Engineering Sciences*, 479(2274):20230076, 2023.

- [11] J. A. Carrillo, X. Chen, Q. Wang, Z. Wang, and L. Zhang. Phase transitions and bump solutions of the Keller–Segel model with volume exclusion. *SIAM Journal on Applied Mathematics*, 80(1):232–261, 2020.
- [12] P. Degond, F. Delebecque, and D. Peurichard. Continuum model for linked fibers with alignment interactions. *Mathematical Models and Methods in Applied Sciences*, 26(02):269–318, 2016.
- [13] P. Degond, M. A. Ferreira, and S. Motsch. Damped Arrow–Hurwicz algorithm for sphere packing. *Journal of Computational Physics*, 332:47–65, 2017.
- [14] P. Degond, A. Frouvelle, and J.-G. Liu. From kinetic to fluid models of liquid crystals by the moment method. *Kinetic and Related Models*, 15(3):417–465, 2022.
- [15] P. Degond, A. Frouvelle, and S. Merino-Aceituno. A new flocking model through body attitude coordination. *Mathematical Models and Methods in Applied Sciences*, 27(06):1005–1049, 2017.
- [16] P. Degond, A. Frouvelle, S. Merino-Aceituno, and A. Trescases. Quaternions in collective dynamics. *Multiscale Modelling & Simulation*, 16(1):28–77, 2018.
- [17] P. Degond, A. Manhart, and H. Yu. A continuum model for nematic alignment of self-propelled particles. *Discrete and Continuous Dynamical Systems - B*, 22(4):1295–1327, 2017.
- [18] P. Degond, A. Manhart, and H. Yu. An age-structured continuum model for myxobacteria. *Mathematical Models and Methods in Applied Sciences*, 28(09):1737–1770, 2018.
- [19] P. Degond and S. Merino-Aceituno. Nematic alignment of self-propelled particles: From particle to macroscopic dynamics. *Mathematical Models and Methods in Applied Sciences*, 30(10):1935–1986, 2020.
- [20] P. Degond, S. Merino-Aceituno, F. Vergnet, and H. Yu. Coupled self-organized hydrodynamics and Stokes models for suspensions of active particles. *Journal of Mathematical Fluid Mechanics*, 21(1):6, 2019.
- [21] P. Degond and S. Motsch. Continuum limit of self-driven particles with orientation interaction. *Mathematical Models and Methods in Applied Sciences*, 18(supp01):1193–1215, 2008.
- [22] L. Dyson and R. E. Baker. The importance of volume exclusion in modelling cellular migration. *Journal of Mathematical Biology*, 71(3):691–711, 2015.
- [23] A. G. Fletcher, M. Osterfield, R. E. Baker, and S. Y. Shvartsman. Vertex models of epithelial morphogenesis. *Biophysical Journal*, 106(11):2291–2304, 2014.
- [24] S. Henkes, M. C. Marchetti, and R. Sknepnek. Dynamical patterns in nematic active matter on a sphere. *Physical Review E*, 97:042605, 2018.
- [25] H. Honda and T. Nagai. Cell models lead to understanding of multi-cellular morphogenesis consisting of successive self-construction of cells. *The Journal of Biochemistry*, 157(3):129–136, 2015.
- [26] S. Ngo, F. Ginelli, and H. Chaté. Competing ferromagnetic and nematic alignment in self-propelled polar particles. *Physical Review E*, 86(5):050101, 2012.
- [27] C. Rackauckas and Q. Nie. Adaptive methods for stochastic differential equations via natural embeddings and rejection sampling with memory. *Discrete and Continuous Dynamical Systems - B*, 22(7):2731–2761, 2017.

- [28] G. Teschl. *Topics in Linear and Nonlinear Functional Analysis*. American Mathematical Society, Providence, 2020. Graduate Studies in Mathematics.
- [29] C. Villani. Limite de champ moyen. *Course de DEA*, pages 1–58, 2001.
- [30] E. G. Virga. *Variational Theories for Liquid Crystals*. Chapman and Hall/CRC, New York, 2019.
- [31] H. Wang and P. J. Hoffman. A unified view on the rotational symmetry of equilibria of nematic polymers, dipolar nematic polymers, and polymers in higher dimensional space. *Communications in Mathematical Sciences*, 6(4):949–974, 2008.
- [32] H. H. Wensink and H. Löwen. Emergent states in dense systems of active rods: from swarming to turbulence. *Journal of Physics: Condensed Matter*, 24(46):464130, 2012.